NASA CONTRACTOR REPORT

NASA CR-62

NASA CR-62

RADIATION DAMAG
SEMICONDUCTORS
ELECTRON AND PR

by John C. Corelli and H.

Prepared under Grant No. NsG-290 *by*
RENSSELAER POLYTECHNIC INSTITUT
Troy, New York
for

NATIONAL AERONAUTICS AND SPACE ADMINI

19710

RADIATION DAMAGE TO SEMICONDUCTORS BY HIGH-ENERGY ELECTRON AND PROTON RADIATION

By John C. Corelli and H. B. Huntington

Prepared under Grant No. NsG-290 by
RENSSELAER POLYTECHNIC INSTITUTE
Troy, New York

NATIONAL AERONAUTICS AND SPACE ADMINISTRATION

For sale by the Office of Technical Services, Department of Commerce,
Washington, D.C. 20230 -- Price $1.75

TABLE OF CONTENTS

I. Introduction

This report covers the research progress made during the six month period 15 March 1963 to 15 September 1963 on the radiation damage program at RPI. Briefly stated, the aims of the research are to investigate the nature of the defects induced in germanium and silicon by high energy electrons 5-60 Mev and protons of about 10 to 130 Mev. The main probes used thus far are the temperature dependence of carrier concentration, conductivity and carrier lifetime. Some room temperature infrared work to investigate the introduction of defect absorption bands has also been performed and the results were presented in our previous progress report (April 1963). The program is sponsored by NASA under Grant NsG-290. A significant portion of the research reported* herein will be prepared in the immediate future for publication in either the Journal of Applied Physics or the Physical Review.

The personnel from RPI directly engaged in the research program during the present year September 1, 1963 to September 1, 1964 are:

1. Faculty

   **Dr. John C. Corelli - 3/4 time 1st semester, full time 2nd semester and summer '64.

   **Dr. H. B. Huntington - part time academic year.

2. Graduate Students

   **Mr. Orrin Merrill - 1/2 time

   **Mr. Charles Taylor - 1/2 time

   Mr. Arne Kalma - 1/2 time

   **Mr. Li-Jen Cheng - 1/2 time

   **Mr. John Fischer - 10 hrs/week (NDEA Fellow, no salary charged to NASA program).

---

* Verbal reports on the results of our research were given by Dr. John C. Corelli (RPI) to personnel at the NASA Langley Research Center, August 26, 1963, and the NASA Lewis Research Center, September 9, 1963.

** Indicates personnel who were engaged in this research program during the past six months and contributed in the preparation of this report.

3. Undergraduate Students - Addition of physics and electrical engineering honors program students will be made during current school year. These students do not receive salary but work on a project as an elective which forms their senior thesis.

Mr. Gordon Oehler - Elect. Eng. Major BSc

II. NASA Switchyard Magnet for RPI Linac

During the past two months the switchyard[+] magnet was installed at the RPI Linac site. The magnet system is capable of deflecting the 10-100 Mev electron beam through angles of $\pm$ 22½° and $\pm$ 45° with respect to the output beam direction of the linac. Intensive tests and experiments on the switchyard system will be performed, and the results will be transmitted to NASA in our next report.

III. 20 to 130 Mev Proton Irradiation of n-Type Germanium

ABSTRACT

Samples of n-type germanium doped with arsenic to nominal resistivities of 1 ohm-cm and 10 ohm-cm were irradiated with 20- to 130-Mev protons at 297°K. Electrical conductivity measurements during bombardment served as an indication of the accumulated damage with proton dose. The dependence of damage on incident proton energy departs markedly from that predicted using coulomb elastic scattering cross-sections and the Kinchin-Pease model for the displacement cascade. Carrier removal rates for 1 ohm-cm material are a factor two larger than for the 10 ohm-cm material. Analysis of the temperature dependence of carrier concentration and Fermi level indicates the presence of defect acceptor level at 0.24 ev below the bottom of the conduction band. Although difficult to resolve, the data strongly suggest the presence of a deep band. Annealing studies indicate stages centered at 75°C and 225°C with all but about 10% of the damage removed by heat treatment to 350°C.

[+]Constructed by the High Voltage Engineering Corp., Burlington, Mass.

A. Introduction

The recent discovery of high-energy protons in the trapped radiation belts has prompted a renewed interest in the general problem of radiation damage to solids. In particular a large amount of effort has been spent on the study of high-energy radiation damage (10-700 Mev protons) to silicon solar cells,[1-2] transistors and other components.[3] A search through the literature indicates that no study has been performed yet on the semiconductor materials per se, eg., silicon, germanium, etc., in the region 10-200 Mev protons.

Although observation of the direct action of high energy radiation on semiconductor device performance has very important practical consideration, it was our feeling that the basic understanding of the actual processes involved in radiation damage could be studied better by working with semiconductor materials per se. For one thing one avoids in this way any complications from junction effects or from changes induced in the component packaging, i.e., transistor cans, etc. Also the radiation damage experiments on solar cells reflect primarily the product of the recombination cross section and the concentration of recombination centers or trapping levels and it is difficult to resolve the influence of each of these parameters separately. On the other hand our measurements of conductivity and Hall coefficient give directly the carrier concentration. Its change with irradiation should reflect directly carrier removal caused by radiation-induced defects. (n=carrier conc., ϕ=integrated flux)

B. Theoretical Considerations

The calculation of the radiation damage which involves a computation of the total number of atomic displacements has been performed[2,4] for protons incident on silicon solar cells up to several hundred Mev. Baicker[4] et al. and Denney[2] et al., were able to obtain fair agreement between the calculated and measured proton-induced radiation damage in silicon. In the energy region of interest in this paper it is necessary to use the actual nuclear scattering data either from experiment or as deduced using the nuclear optical model rather than purely Rutherford scattering cross sections. This fact arises from (the pronounced departures of the scattering from coulombic and) the necessity of invoking nuclear interaction potentials in addition to the coulomb potential to compute the scattering cross-sections. A very recent discussion of the optical model for analysis of proton elastic scattering has been given by Perey[5] in which spin-orbit interaction potentials are also taken into account.

The general method for calculating the total number of displaced atoms by protons per unit path in germanium can be computed in a straight forward manner under the following assumptions,

1) Sample thickness is very small compared to the range of the incident particle.

2) Neglect annealing of displaced atoms. Under the approximations inherent in the assumptions (1) and (2) one has

$$N_d = \int_{E_d}^{E_m} n_0 g(E) \left\{ \frac{d\sigma_0(E)}{dE} + \sum_{i=1}^{p} \frac{d\sigma_i(E)}{dE} + \sum_{i \neq j} \frac{d\sigma_{i,j}(E)}{dE} \right\} dE \qquad (1)$$

where N_d is the number of displacements per unit path, E_m is the maximum recoil energy imparted to a germanium nucleus by a proton of incident energy E_p, E_d is the threshold energy for producing a displaced atom ($\sim$ 15-30 ev for germanium), N_0 is the number of germanium atoms per cm^3, E is the energy of the primary knock-on, $\frac{d\sigma_0(E)}{dE}$ is the cross-section for energy transfer to the germanium nucleus by the elastic scattering process, $\sum \frac{d\sigma_i(E)}{dE}$ is the cross-section for energy transfer to germanium nucleus in its first excited state (i=1), its second excited state (i=2) etc., $\sum_{i \neq j} \frac{d\sigma_{i,j}(E)}{dE}$ is the cross section for energy transfer to the germanium nucleus by nuclear reactions of the type (p,n), (p,d), (p,2p), (p,2n), + - - -. The cross-sections for the so-called spallation reactions would be included in this summation. The quantity g(E) is the total number of atoms displaced by a primary knock-on energy E. The forms used for g(E) by various authors[4,6] differ slightly from that derived by Kinchin and Pease.[7]

In some recent work by Oen and Robinson[8] a "channeling" mechanism of energetic atoms is proposed to refine the displacement cascade theory, particularly for fcc lattice types. Briefly, the channeled atom idea allows energy of the primary to be dissipated by glancing collisions without producing displaced atoms. Once in a channel the atom motion is stable since the glancing collisions constrain the moving atom. The high value of N_d computed, relative to experimentally determined number of total displacements is believed to be due to the overestimate of the number of displacements made by a primary, i.e., g(E). The work of Oen and Robinson[8] appears to be a promising approach if all other quantities in Equation (1) above are known. It must also be realized that for the 10 to 20 Mev energy region the cross sections appearing in eq.(1) are all small compared to the elastic scattering, and do not have to be included in the computation.

The cross-sections appearing in equation (1) which pertain to germanium have not been measured, and for this reason we have not attempted to calculate N_d. However, it might be possible to use the predictions of the nuclear optical model to extrapolate the relevant cross-sections that have been measured[9] for nuclei like copper, zinc and nickel and apply them to germanium. This procedure was not considered worthwhile at the present time.

The energy dependence of the calculated number of displacements N_d (from eq. 1) can be compared to the measured carrier removal rate $\frac{dn}{d\phi}$ vs. E, where E is the incident proton energy n and ϕ have the meaning previously assigned them. It is important to measure the integrated flux accurately (better than 5% if possible) in order to make meaningful comparisons between the theory and experiment. The difficulty in deciding whether one or two carriers are removed per displaced atom can be avoided by normalizing the theoretical and experimental values at one energy and comparing the shapes of the resulting curves of $\frac{dn}{d\phi}$ vs. E and N_d vs. E.

It is to be borne in mind that equation (1) will always tend to overestimate the damage for germanium bombarded at room temperature because of the well known low temperature annealing.[10] In order to take into account annealing then one would have to decrease N_d computed from eq. (1) by an amount which depends on the annealing kinetics from about 20°K to 300°K, and activation energy for defect motion. More precisely, equation (1) should be applied to the introduction rates of one type of defect as characterized by the defect energy level being introduced in the forbidden gap at the irradiation temperature.

C. Experimental Methods

Commercially available† single crystal germanium ingots doped with arsenic to nominal resistivities of 1- and 10 ohm-cm were cut into wafers 30-40 mils thick. Variations from the nominal resistivity due to inhomogeneity were ± 20%. A standard ultrasonic cutter** was used to fabricate 6-arm bridge samples from the discs. The

† Semi Metals Inc., Westbury, L.I.

** Samples were cut at the Instrument Research Division, NASA Langley Research Center, Hampton, Virginia.

bridge samples were polished and etched in CP-4 to the desired thickness (~20-25 mils). Hall, resistivity and current leads were attached to the arms using an indium alloy solder. The Hall and resistivity voltages were measured using either a Leeds and Northrup K-3 potentiometer or a Non-Linear-Systems precision digital voltmeter.

The irradiations were performed at the Harvard University 160-Mev proton cyclotron. The energy of the proton beam was degraded using aluminum absorbers. The sample temperature during irradiation was never higher than 24°C. The proton flux was measured using an ionization chamber calibrated against a Faraday Cup. Beam spread due to straggling in the aluminum absorbers was measured by traversing the beam spot (1½" nominal diameter) with a 20-mil square silicon diode. The ionization current from the ion pairs produced in the silicon diode was fed to a standard current integrator. The silicon diode was pre-damaged by protons and was found to give very reproducible results thereafter. The flux variation over the irradiated portion of the sample was less than 5%, and the overall accuracy of our absolute flux determination is better than 10%.

The parameter measured during irradiation was the conductivity. The post irradiation temperature dependence of carrier concentration and conductivity in addition to the results of the annealing measurements are not yet complete. The results will be given in a forthcoming publication, and only preliminary results will be discussed in a later section of this paper.

D. Experimental Results

The decrease in conductivity with proton flux at various incident proton energies for 1 ohm-cm (nominal) n-type arsenic-doped germanium is shown in Figures 1 and 2. Apart from some scatter in sample number 138 the decrease appears to be quite linear for all samples investigated. Similar results for 10 ohm-cm (nominal) n-type arsenic-doped germanium are given in Fig. 3, in which conductivity is plotted as a function of flux for the various incident proton energies. The decrease in conductivity with flux is linear for all samples over the proton flux range studied, except for sample number 126 where a bend is observable near a flux of 1.7×10^{12} p/cm^2. This bend is normally observed just before germanium becomes intrinsic and converts to p-type with further irradiation. It can be seen from Fig. 3 that sample number 126 has incurred the largest change in conductivity, and further irradiation would have driven the sample to its intrinsic state.

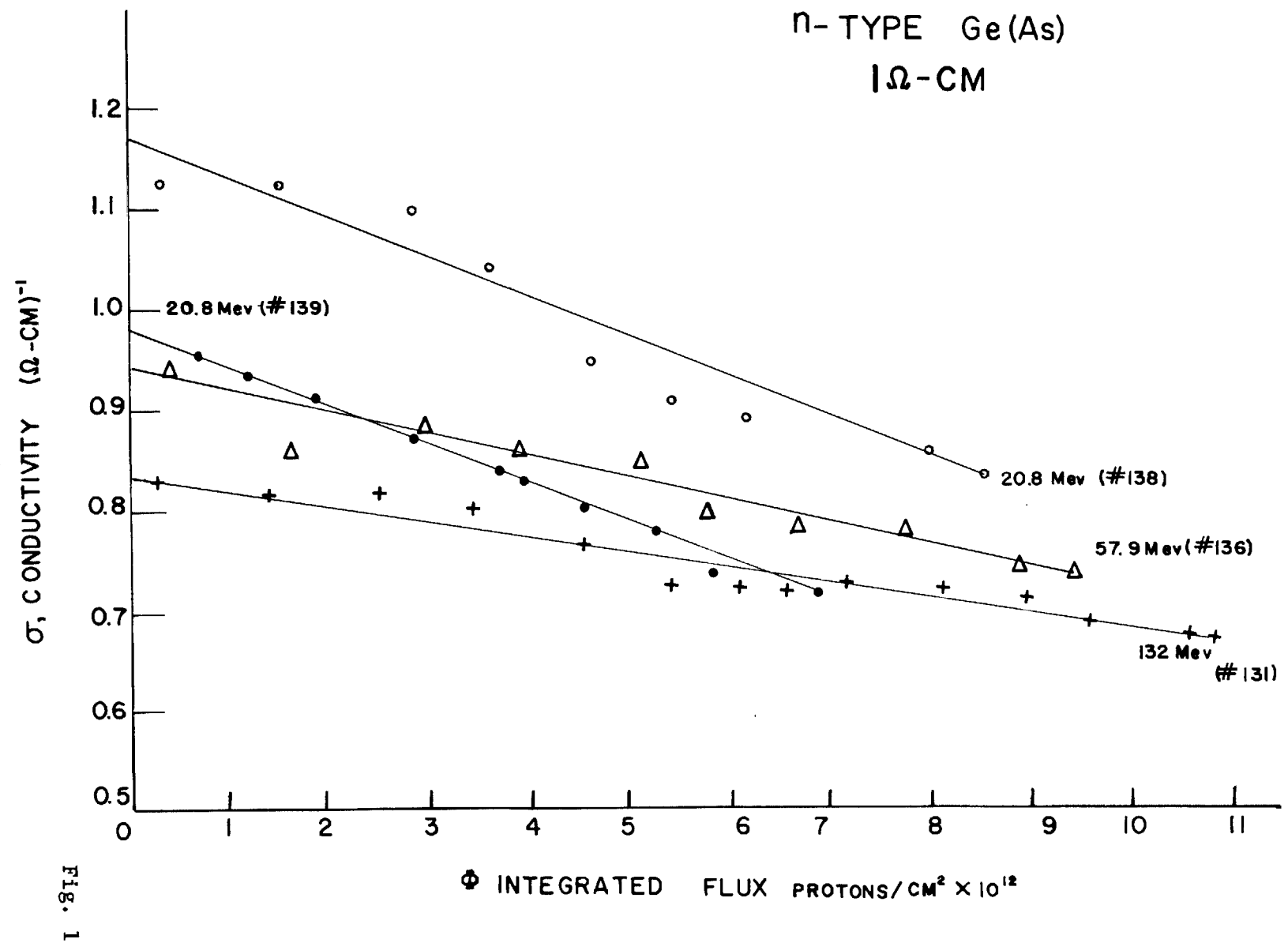
n- TYPE Ge(As)
1Ω-CM
σ, CONDUCTIVITY (Ω-CM)⁻¹
1.2
1.1
1.0
0.9
0.8
0.7
0.6
0.5
20.8 Mev (#139)
20.8 Mev (#138)
57.9 Mev (#136)
132 Mev (#131)
0
1
2
3
4
5
6
7
8
9
10
11
Φ INTEGRATED FLUX PROTONS/CM² X 10¹²

Fig. 1

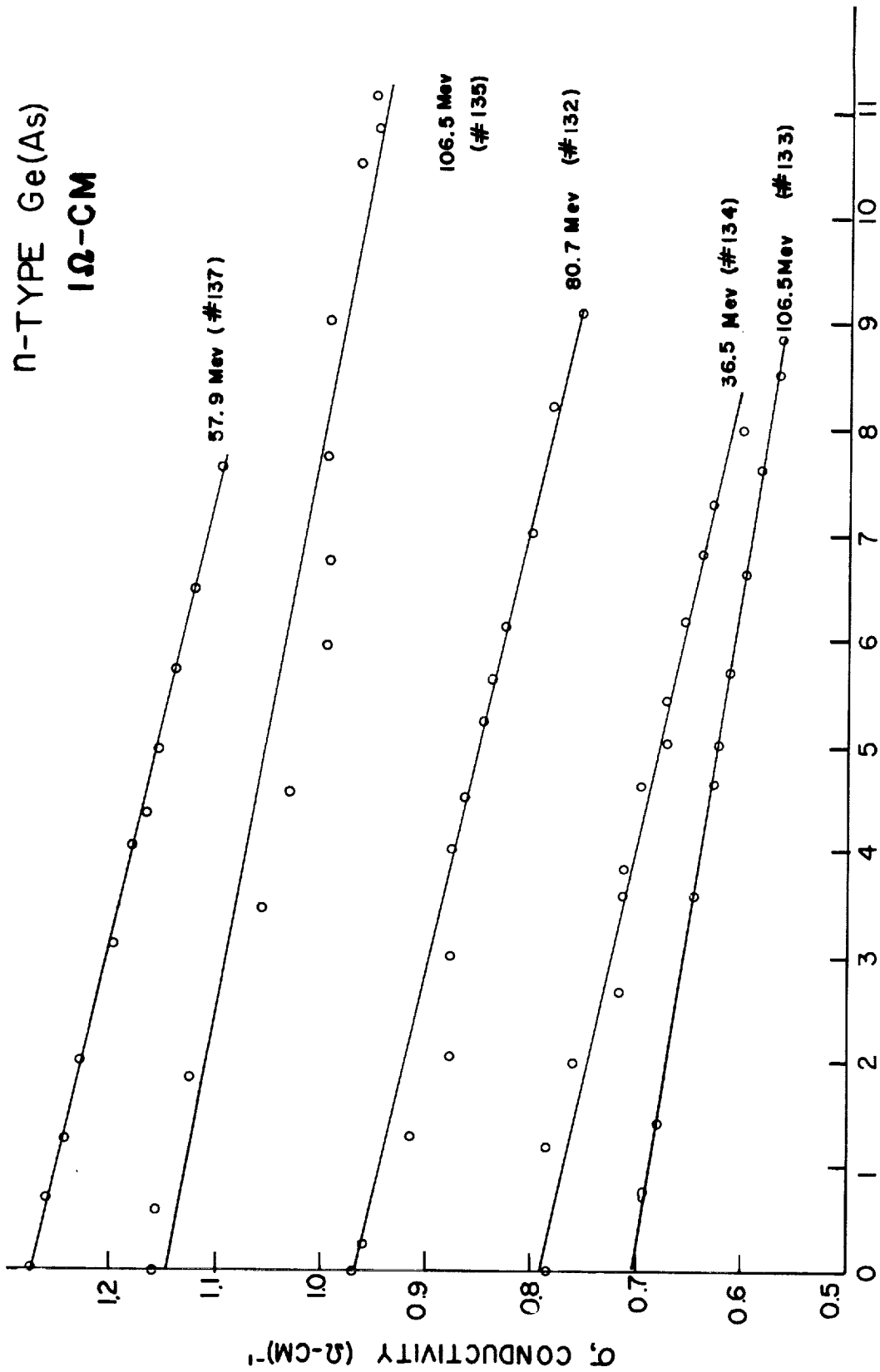
n-TYPE Ge(As)
1Ω-CM
57.9 Mev (#137)
106.5 Mev (#135)
80.7 Mev (#132)
36.5 Mev (#134)
106.5Mev (#133)
σ, CONDUCTIVITY (Ω-CM)⁻¹
Φ INTEGRATED FLUX PROTONS / CM² X 10¹²
0.5
0.6
0.7
0.8
0.9
1.0
1.1
1.2
0
1
2
3
4
5
6
7
8
9
10
11

Fig. 2

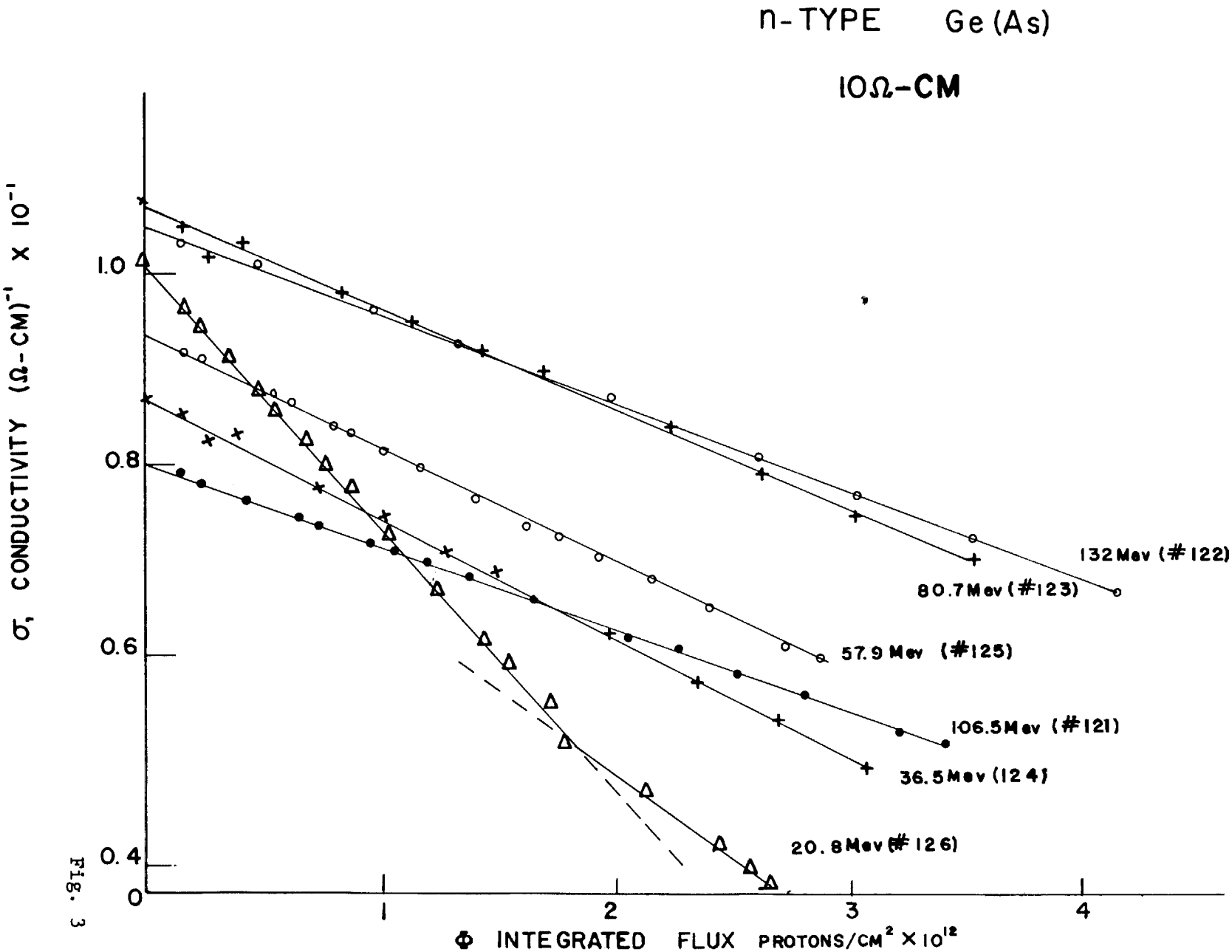
n-TYPE Ge (As)
10Ω-CM
σ, CONDUCTIVITY (Ω-CM)⁻¹ X 10⁻¹
1.0
0.8
0.6
0.4
0
1
2
3
4
Φ INTEGRATED FLUX PROTONS/CM² X 10¹²
132 Mev (#122)
80.7 Mev (#123)
57.9 Mev (#125)
106.5 Mev (#121)
36.5 Mev (124)
20.8 Mev (#126)

Fig. 3

The data of figures 1, 2, and 3 were calculated to yield radiation damage vs. energy curves as follows. The quantity $\frac{\sigma_o - \sigma}{\sigma_o}$ was computed at an integrated proton flux of 6×10^{12} p/cm^2 for each of the samples given in figures 1 and 2. Note, σ_o is the initial conductivity and σ is the conductivity after the sample was subjected to a dose of 6×10^{12} p/cm^2. The results of the "damage" vs. energy plot are shown in Fig. 4 for the 1 ohm-cm germanium samples. A similar calculation was made for the data on the 10 Ω-cm samples given in Fig. 3. The damage vs. proton energy curve for the 10 Ω-cm samples is shown in Fig. 5.

In view of the linear decrease of conductivity with flux (see Figs. 1, 2, and 3) and the very small change in mobility after irradiation as compared to the carrier concentration decrease the data shown in Figures 1, 2, and 3 were utilized to calculate carrier removal rates for these extrinsic samples from

$$\frac{\Delta\sigma}{\Delta\phi} = \mu e \frac{\Delta n}{\Delta\phi}$$ where

n is the carrier concentration, σ is the conductivity, e is the electron charge, μ is the mobility and ϕ is the integrated proton flux. The carrier removal rates for the 1 and 10 ohm-cm samples bombarded by various proton energies are given in Table I.

TABLE I

Experimentally determined values of carrier removal rate n-type germanium (arsenic doped) at various incident proton energies (σ_o and R_{H_o} are the conductivity and Hall coefficient respectively before irradiation).

Sample Number	Proton Energy (Mev)	σ_o (ohm-cm)$^{-1}$	R_{H_o} $\frac{cm^3}{coul}$	$\frac{\Delta n}{\Delta\phi}$ carrier/proton/cm
131	132	0.857	4.1×10^4	30
132	81	0.952	4.3	47
133	107	0.757	4.2	39
134	37	0.810	4.2	46
135	107	1.18	2.8	33
136	58	0.942	3.4	46
137	58	1.29	2.5	43
138	21	1.22	3.0	68
139	21	.985	3.3	81
121	107	.0812	4.0×10^5	15
122	132	0.111	3.6	16
123	81	0.108	3.4	18
124	37	0.867	4.1	22
125	58	0.960	3.4	20
126	21	0.104	3.4	47

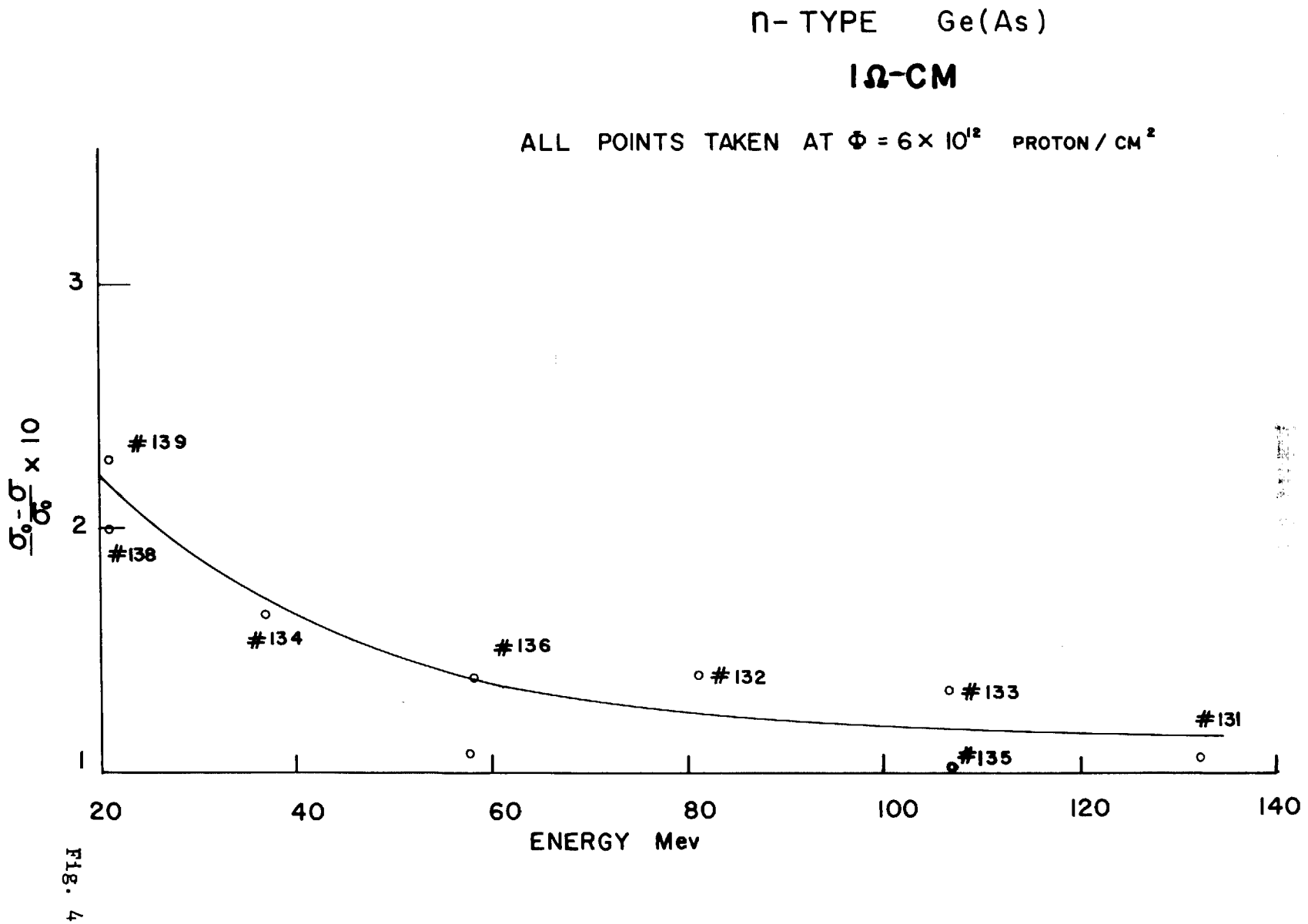
n- TYPE Ge(As)
1Ω-CM
ALL POINTS TAKEN AT Φ = 6 × 10^12 PROTON / CM^2
$\frac{\sigma_o - \sigma}{\sigma_o} \times 10$
3
2
1
#139
#138
#134
#136
#132
#133
#131
#135
20
40
60
80
100
120
140
ENERGY Mev

Fig. 4

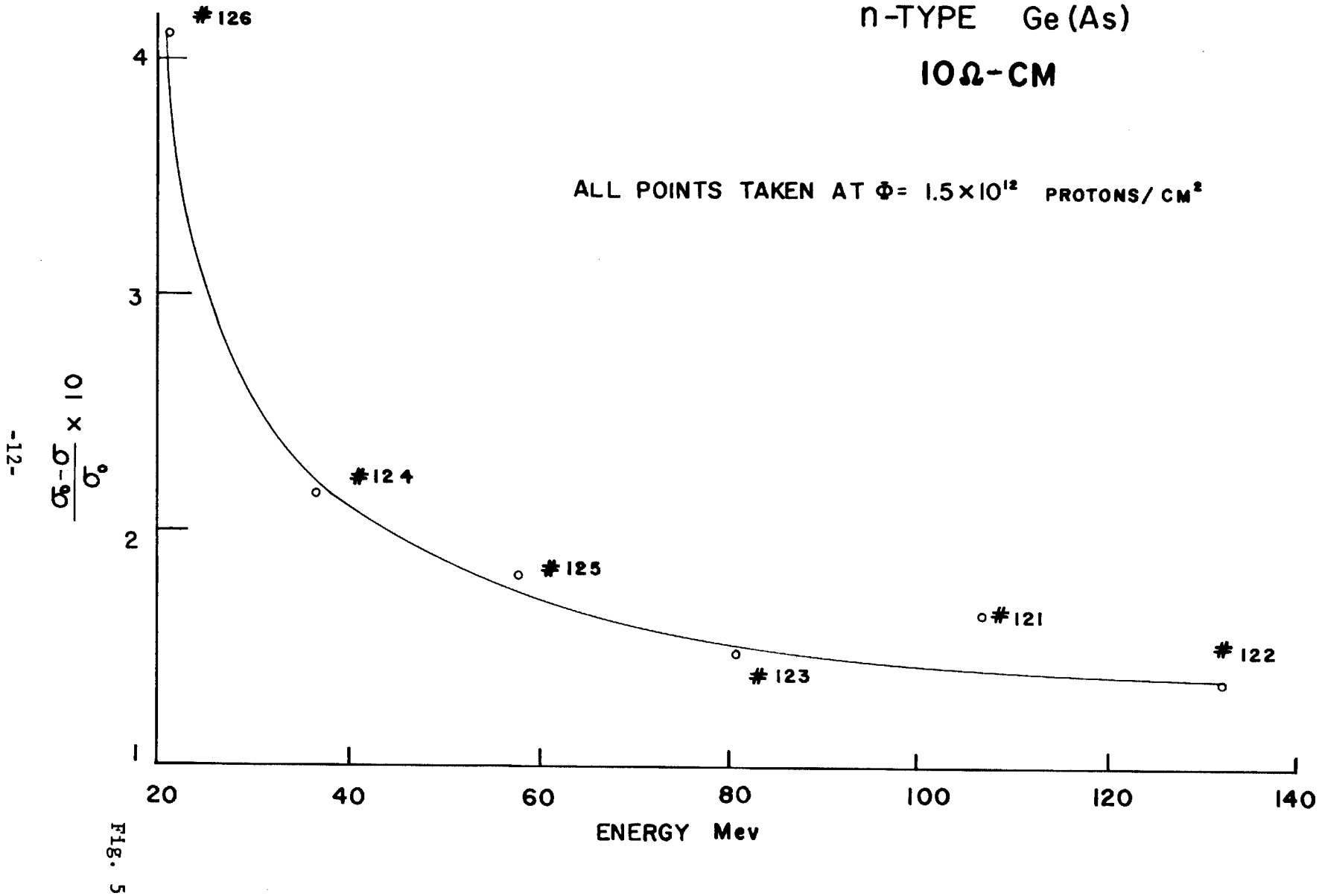
n-TYPE Ge (As)
10Ω-CM
ALL POINTS TAKEN AT Φ= 1.5×10¹² PROTONS/ CM²
#126
#124
#125
#121
#122
#123
4
3
2
1
20
40
60
80
100
120
140
ENERGY Mev
$\frac{\sigma-\sigma_0}{\sigma_0} \times 10$

Fig. 5

E. Discussion of Results and Conclusions

Using simple theory* for calculating the approximate number of total displacements as a function of energy the comparison with the measured values is shown in Fig. 6. An immediate conclusion evident from Fig. 6 is that at proton energies larger than about 30 Mev marked departures between experiment and theory are evident. This departure can be attributed in most part to neglect of nuclear elastic and inelastic scattering processes in the cross section used in Fig. 1. The comparison shown in Fig. 6 is intended to point out the necessity of including important non-elastic events between the proton and germanium in the energy region 30-130 Mev. Otherwise it can be concluded that the results in Fig. 6 are roughly what one would expect from damage vs. proton energy for semiconductors.

In order to obtain an approximate idea of the nature of the damage Rutherford scattering was used to calculate the mean free path of protons between displacement collisions. The mean free path calculated in this manner, 10^{-2} cm, is one fifth the sample thickness used in the experiments, 5×10^{-2} cm, thus implying widely separated heavily damaged regions ("clusters" of defects) in the crystal.

F. Temperature Dependence and Annealing

We wish to discuss the highlights of our post-irradiation temperature dependence and annealing measurements that have thus far been completed on 2 one ohm-cm samples (#137 and #133) and 2 ten ohm-cm couples (#122 and #126). The results of isochronal annealing experiments on a 1 Ω cm and two 10 Ω-cm samples are shown in Figs. 7 and 8 respectively. Isochronal annealing experiments on Hall coefficient and conductivity measurements for 10 ohm-cm specimens indicate annealing stages centered at 75°C and 225°C with about 10% of the damage remaining after warmup to 350°C. The samples were heated in a helium atmosphere to various temperatures from 50°C to 350°C for 45 minute intervals, and subsequently remeasured from 75°K up to room temperature before and after each anneal. It is significant to compare these annealing results with those observed

---

* The Rutherford elastic scattering cross-section and Kinchin-Pease model for computing the total number of displacements are used in equation (1). Annealing has been neglected.

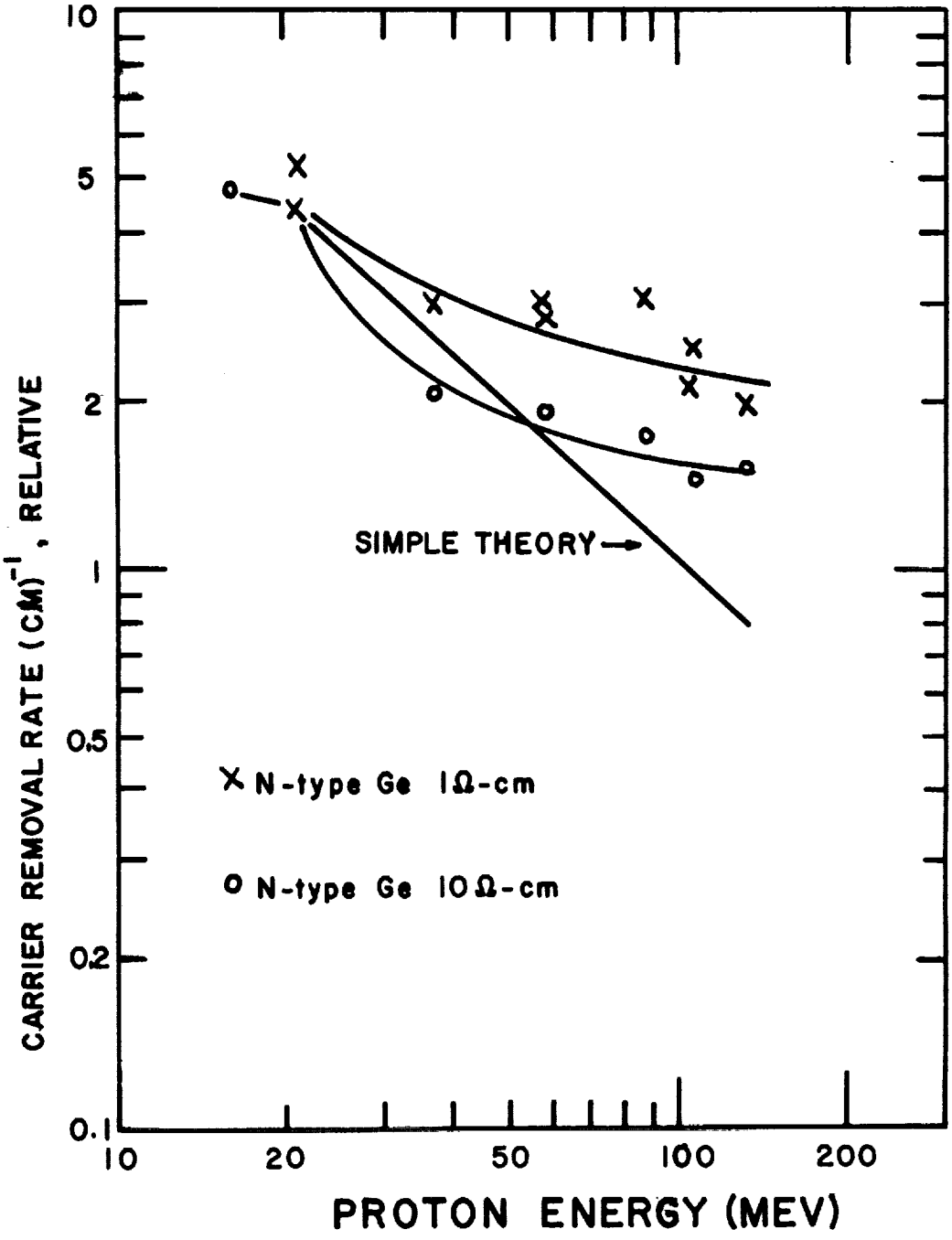
10
5
2
1
0.5
0.2
0.1
10
20
50
100
200
CARRIER REMOVAL RATE (CM)$^{-1}$, RELATIVE
PROTON ENERGY (MEV)
SIMPLE THEORY
X N-type Ge 1Ω-cm
O N-type Ge 10Ω-cm

Fig. 6

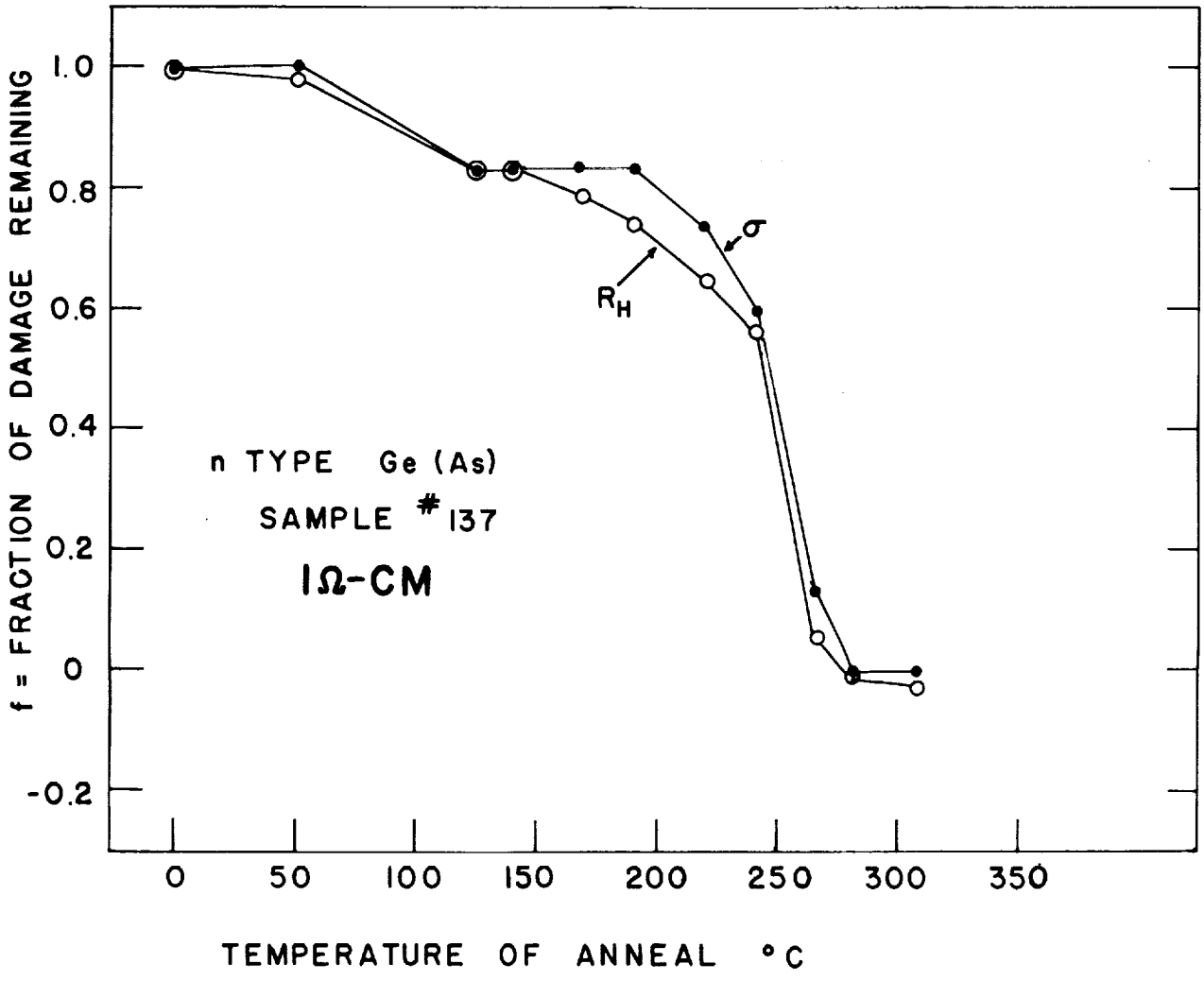
f = FRACTION OF DAMAGE REMAINING
1.0
0.8
0.6
0.4
0.2
0
-0.2
n TYPE Ge (As)
SAMPLE # 137
1Ω-CM
R_H
σ
0
50
100
150
200
250
300
350
TEMPERATURE OF ANNEAL °C

Fig. 7

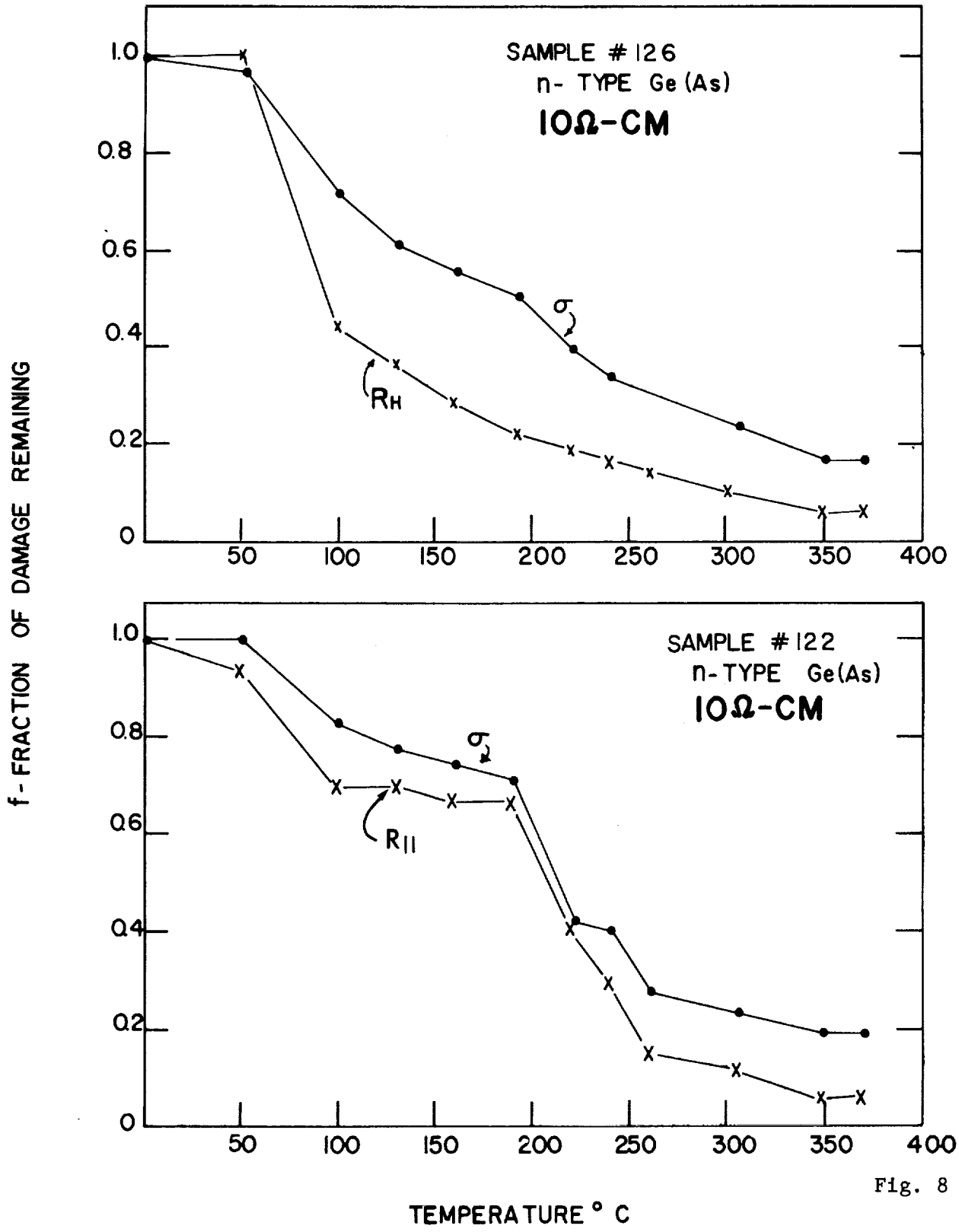
SAMPLE # 126
n- TYPE Ge (As)
10Ω-CM
σ
R_H
SAMPLE # 122
n-TYPE Ge(As)
10Ω-CM
σ
R_{II}
f - FRACTION OF DAMAGE REMAINING
TEMPERATURE ° C
1.0
0.8
0.6
0.4
0.2
0
50
100
150
200
250
300
350
400

Fig. 8

in arsenic-doped germanium irradiated with Co^{60} gamma rays. O. L. Curtis and J. H. Crawford [11] measuring minority carrier lifetime observed annealing stages at $\sim$85°C and 230°C, while Ishino et al.[12], measuring conductivity and Hall effect observed predominant annealing stages at $\sim$ 147°C and 252°C.

Before and after each anneal temperature dependence measurements of conductivity and carrier concentration were made. The temperature dependence of carrier concentration and Fermi level indicate the presence of an acceptor level 0.24 ev below the bottom of the conduction band, (see Fig. 9) which anneal out completely after heat treatment to 221°C. The measurements also suggest the presence of a deep level greater than 0.3 ev below the bottom of conduction band. The carrier concentration dependence on temperature after successive anneals is shown in Fig. 9 where Hall coefficient is plotted vs. $\frac{1000}{T(^{o}K)}$. It was not possible to resolve this deep level from the measurements made. The defect energy levels which we have found are indeed very similar to those observed for germanium bombarded with 10 Mev deuterons and reported by H. Y. Fan[13]. In summary then we conclude that 20-130 Mev proton bombardment of germanium produces damage which in many respects is similar to what has been observed for low-energy gammas, deuterons, etc. Moreover we feel that the expected highly complex damage is not very much different than what is observed at low energies. Further experiments will undoubtedly prove fruitful in understanding high-energy damage and is the subject of a continuing program in our laboratory.

Acknowledgement - The kind assistance of Mr. Andy Koehler of the Harvard Cyclotron in measuring the proton flux and his general overall aid with the bombardments is gratefully acknowledged.

The assistance of Mr. David Golibersuch in setting up the apparatus and making the measurements was crucial in temperature dependent experiments. Finally, the assistance of Instrument Research Division Personnel at NASA Langley Research Center, Hampton, Virginia, is acknowledged.

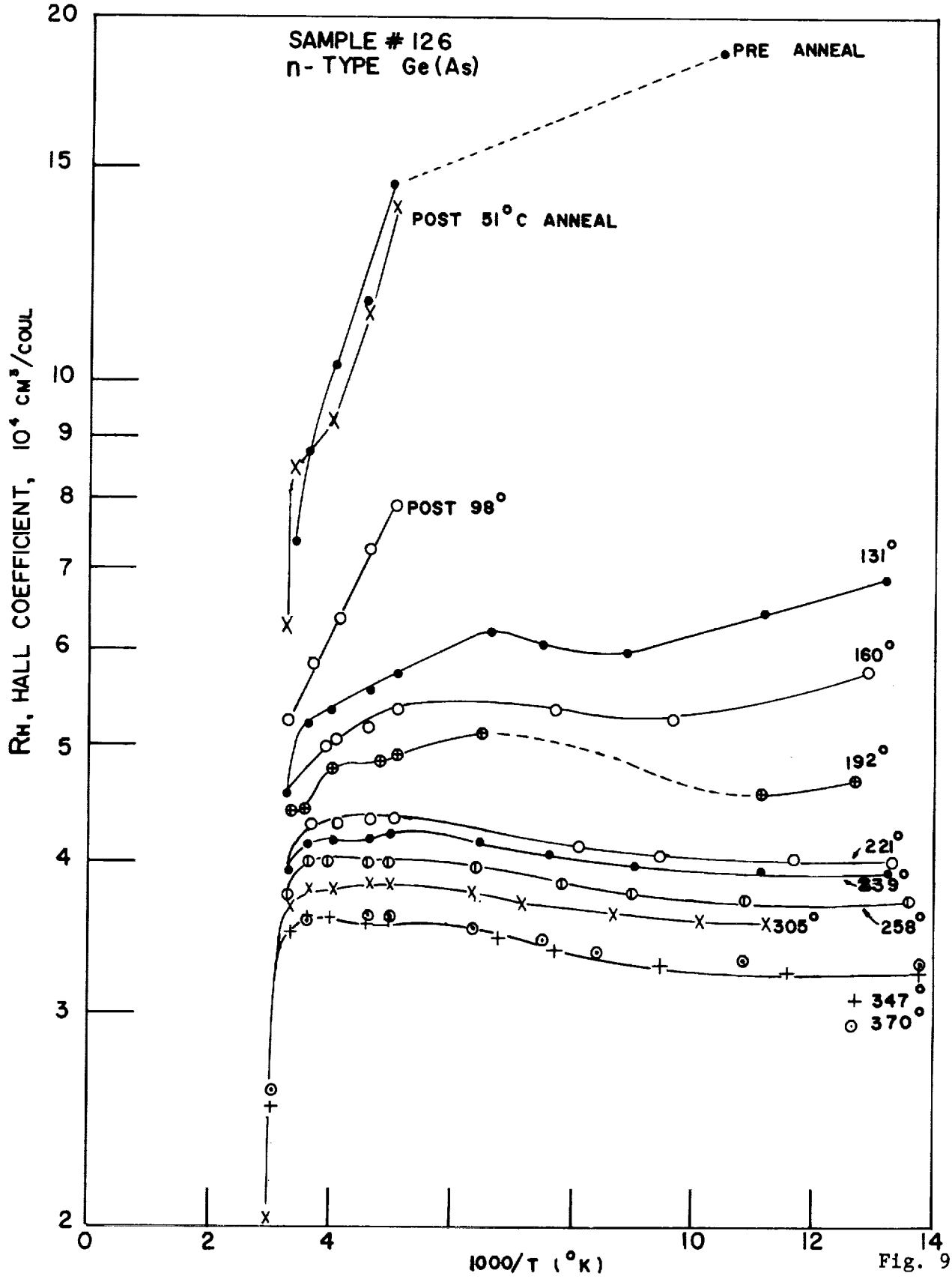
SAMPLE # 126
n-TYPE Ge(As)
PRE ANNEAL
POST 51°C ANNEAL
POST 98°
131°
160°
192°
221°
239°
258°
305°
347°
370°
RH, HALL COEFFICIENT, 10⁴ CM³/COUL
1000/T (°K)
20
15
10
9
8
7
6
5
4
3
2
0
2
4
10
12
14

Fig. 9

G. Figure Captions

Fig. 1 Conductivity vs. Integrated Flux for Four of the 1 ohm-cm Arsenic-Doped Germanium Samples at Various Proton Energies

Fig. 2 Conductivity vs. Integrated Flux for Five of the 1 ohm-cm Arsenic-Doped Germanium Samples at Various Proton Energies

Fig. 3 Conductivity vs. Integrated Flux for Six 10 ohm-cm Arsenic-Doped Germanium Samples at Various Proton Energies

Fig. 4 Percentage Change in Conductivity (i.e., Radiation Damage) vs. Proton Energy for Arsenic-Doped 1 ohm-cm Germanium

Fig. 5 Percentage Change in Conductivity (i.e., Radiation Damage) vs. Proton Energy for Arsenic-Doped 10 ohm-cm Germanium

Fig. 6 Comparison of the Measured Carrier Removal Rate N_d for 1 and 10 ohm-cm n-Type Germanium with the Values Calculated from Simple Theory using Rutherford Scattering and the Kinchin-Pease Model, Measured and Calculated Points have been Normalized at 20 Mev.

Fig. 7 Isochronal Annealing Results on a 1 Ω-cm n-Type Ge Sample Irradiated with 58 Mev Protons. (σ , R_H are the conductivity and Hall coefficient respectively).

Fig. 8 Isochronal Annealing Results on Two 10 Ω-cm n-Type Ge Samples Irradiated with 21 Mev (sample #122) and 132 Mev (sample #126) Protons. (σ , R_H are the conductivity and Hall coefficient respectively).

Fig. 9 Temperature Dependence of Hall Coefficient after Successive 45 Minute Anneals at the Indicated Temperatures for a 10 Ω-cm n-Type Ge Irradiated with 21 Mev Protons.

H. References

1. F. W. Smits, W. Rosenzweig, and W. L. Brown, Proc. Solar Working Group Conference 27 and 28 February 1962, Vol. 1, PIC-SOL - 209/2.

2. G. W. Simon, J. M. Denney, and R. G. Downing, Phys. Rev. 129, 2454 (1963).

3. W. C. Honaker, "The Effects of Protons on Semiconductor Devices", Proc. of the Symposium on the Protection Against Radiation Hazards in Space, Conference held in Gatlinburg, Tennessee, November 5-7, 1962, TID-7652. Other relevant papers are contained therein.

4. J. A. Baicker, H. Flicker, and J. Vilms, Appl. Phys. Letters 2, No. 5, 104 (1963).

5. F. G. Perey, Phys. Rev. 131, 745 (1963). Earlier references are cited in Perey's paper.

6. F. Seitz and J. S. Koehler, Solid State Physics, Vol. 2, p. 381, 382, (1956).

7. G. H. Kinchin and R. S. Pease, Reports on Prog. in Phys. (Phys. Soc., London 1955) Vol. 18, p. 1. In this paper Kinchin and Pease give

$$g(E) = 0 \quad \text{for} \quad E < E_d$$

$$g(E) = 1 \quad \text{for} \quad E_d \leq E \leq 2\,E_d$$

$$g(E) = \frac{E}{2E_d} \quad \text{for} \quad E > 2\,E_d$$

8. O. S. Oen and M. T. Robinson, Appl. Phys. Letters 2, 83 (1963).

9. W. W. Devins, H. H. Forester, and G. G. Gigas, Nuc. Phys. 35, 6-7 (1962) (30.8 Mev protons).
A. E. Taylor and E. Wood, Nucl. Phys. 25, 642 (1961) (140 Mev protons).
F. G. Perey, Phys. Rev. 131, 745 (1963) (9-22 Mev protons).
G. Gerstein, J. Niederer, and K. Strauch, Phys. Rev. 108, 427 (1957) (96 Mev protons).
N. Hintz, Phys. Rev. 106, 1201 (1957) (10 Mev protons).
N. Hintz, Bull. Am. Phys. Soc. Ser. II, 2, 14 (1957) (40 Mev protons).

References
(Cont'd)

10. J. W. McKay and E. F. Klontz, J. Appl. Phys. 30, 1269 (1959) W. L. Brown, W. M. Augustyniak and T. R. Waite, J. Appl. Phys. 30, 1258 (1959).

11. O. L. Curtis, Jr. and J. H. Crawford, Jr., Phys. Rev. 126, 1342 (1962).

12. S. Ishino, F. Nakazawa, and R. R. Hasiguti, J. Phys. Chem. Solids, 24, 1033 (1963).

13. H. Y. Fan and K. Lark-Horovitz, "The Effects of Radiation on Materials" edited by J. J. Harwood et al., Reinhold, p. 159, (1958).

IV. 10 to 50 Mev Electron Irradiation of Silicon and Germanium

ABSTRACT

Defects induced in germanium (1 to 40 Ω-cm) and silicon (1 to 10 Ω-cm) at room temperature by 10 to 50 Mev electrons were detected by Hall effect and conductivity measurements. Minority carrier lifetime studies were also used to detect damage for the germanium samples. The carrier removal rates measured for n-type silicon of 10 Ω-cm were larger and increased more rapidly with electron energy than do those of 10 Ω-cm p-type silicon. The measured carrier removal rates for n-type germanium are in general about 50 to 100 times larger than values measured for similar resistivity p-type germanium. Analysis of carrier lifetime measurements made on electron irradiated germanium strongly suggest the presence of a single radiation-induced trapping level for the 10 Mev bombardments but at 54 Mev the situation is still obscure. We used the Mott-McKinley-Feshbach scattering cross sections and the Kinchin-Pease model for the total number of displacements caused by the primary knock-on. Fair agreement with the shape of the measured damage for n-type silicon and germanium vs. energy curves is obtained. An irradiation of 10 Ω cm n-type silicon and 1 Ω cm p-type germanium at -146°C by 40 Mev electrons indicate 1) no annealing occurs for silicon from -146°C up to 25°C, 2) defect levels are introduced at about 0.16 ev and 0.4 ev below the bottom of the conduction bank in silicon, 3) for p-type germanium an annealing stage is observed at about 200°K.

IV. 10 to 50 Mev Electron Irradiation of Silicon and Germanium

A. INTRODUCTION

This section of the report will deal with recent results obtained in the electron (10-54 Mev) irradiation of n- and p- type silicon and germanium. The production and nature of the defects were studied as a function of electron energy from 10 to 54 Mev using Hall effect, conductivity and minority carrier lifetime as the measurement probes. Analysis and tentative conclusions reached thus far will be included.

The use of carrier concentration and conductivity temperature dependence for studying radiation damage in semiconductors are well established techniques and require no further comment as far as this report is concerned. The sensitivity of excess carrier recombination kinetics to radiation-induced defects has been established by many investigators.(1) Measurements of electrical properties which are directly related to minority carrier lifetime have led to the establishment of experimental values for E_{b_o}, the minimum incident electron energy required to produce a lattice defect, for Ge and Si.(2) Information concerning the charge states of radiation-induced levels in the forbidden gap can be obtained by determining the capture cross-sections of the defect for minority holes and electrons.(1)

The section of this report dealing with minority carrier lifetime is a preliminary summary of a program having the following objectives:

i) to determine the functional form of (E_b), the probability of forming a defect as a function of electron bombardment energy

ii) to determine, insofar as possible, the nature of the defect as a function of energy

iii) to separate the effect on recombination kinetics of chemical impurities and of radiation-induced defects so that measurement of τ, σ, and R_H can be meaningfully applied in unison to radiation damage (τ, minority carrier lifetime σ, conductivity and R_H, Hall coefficient).

iv) to study the temperature dependence of τ, including the annealing kinetics and characteristics.

B. EXPERIMENTAL PROCEDURE

The samples used for resistivity and Hall measurements were in the form of bridges of approximate thickness .025 inches. Electroless nickel plating[3] was used as a technique for making ohmic electrical contacts to the samples. Leads were soldered to the nickel plate using a silver eutectic solder.

The samples[++] used for lifetime measurements were cut from single crystals of germanium to 2mm x 2mm x 18 mm, polished in three stages ending with 4/0 emery paper and etched for one minute in white etch (3 parts HNO_3 to 1 part HF). The sample size used is considered the optimum compromise between minimizing surface recombination effects and producing homogeneous damage. Leads were applied directly using silver eutectic solder.

Samples were irradiated with electrons of energies from 10 Mev to 56 Mev using the pulsed RPI Microwave Linear Accelerator. The electron pulses varied from 0.3 to 4.5 μsec width; peak beam current was of the order of 40 ma, and rates of 15 to 60 pulses/sec were used. The sample temperature rise was thus kept less than $4C^{o}$ for the bridge samples and below $1C^{o}$ for the larger lifetime samples. The energy resolution of the Linac beam was estimated as $\frac{\Delta E}{E}$ less than 10% at the low beam currents employed in these experiments.

Beam current was measured with an aluminum Faraday cup located behind the sample-holding apparatus. The beam was shaped by a 5" long aluminum collimator and the beam area was determined by darkening a sheet of clear polyvinyl acetate plastic. This method will shortly be replaced by scanning the beam spot with a thermocouple embedded in a 80-120 mil diameter copper sphere mounted on an x-y traversing microscope stage. Measurement of electron flux is currently our largest source of error (about 25%), which can only be ascertained by the scanning technique. We anticipate reducing the error in flux to 5% or less.

A two-inch electromagnet with a hole in the pole pieces was used for making Hall coefficient measurements. During irradiation the beam was allowed to pass through the hole in the magnet, and the sample was placed between the pole pieces at right angles to the beam. A 5-inch aluminum collimator was used to confine the beam area to a size less than that of the hole in the pole pieces. Measurements of the conductivity and Hall coefficient were made as a function of the integrated electron flux.

[++] Single crystal germanium was obtained from Semi Metals Inc., Westbury, L.I. Some of the germanium was kindly given to us by Dr. H. Y. Fan, Physics Department, Purdue University, Lafayette, Indiana. The silicon was obtained from Merck Co., Rahway, N. J.

Lifetime was measured at room temperature by observing the decay of photoconductivity.[4,5] The steady-state sample current and the intensity of the pulsed light were kept small. The p-type examples (irradiated at room temperature in May 1963) were removed from the target room after each dose and measured in an adjacent laboratory. In addition to being inefficient, this procedure led to scatter in the data, caused by differing alignments for each dose. The n-type samples were irradiated (also at room temperature) two months later, with lifetime measurements made remotely with the sample in situ. Pulsed light was incident at a 45° angle to the beam direction at all times. Lifetimes were measured with the beam off. The equipment used consisted of: Tektronix type 1121 amplifier (used only on 3.5 Ω-cm), Tektronix type 564 storage oscilloscope and a General Radio Strobotac, using an EGG FX-6A xenon flashtube (0.8 μsec pulse duration, 210,000 candlepower) operated at 70 pulses/sec.

Lifetime was monitored continuously during each bombardment, but noise from the electron beam made accurate measurement impossible. Room-temperature annealing was observed to an extent of 5% and was subsequently ignored. Changes in conductivity could also be observed by monitoring the pulse height.

Total fluxes varied from 3×10^{13} to 7×10^{14} e/cm^2 depending on initial resistivity. Initial lifetimes in germanium varied from sample to sample; typical values were: 10 Ω-cm p-type, 130 μsec; 3.5 Ω-cm n-type, 80 μsec; 20 Ω-cm n-type, 80 μsec; 40 Ω-cm n-type, 700 μsec. Apparently the 10 Ω-cm and 20 Ω-cm ingots had large concentrations of imperfections prior to irradiation since the lifetime is lower than expected from other similar work.[4]

One 10-ohm-cm bridge sample of phosphorous-doped n-type Si and one 1-ohm-cm bridge sample of Ga-doped p-type Ge were irradiated simultaneously in a liquid nitrogen cryostat** at a temperature of -146°C with 40.5 Mev electrons. The samples were located in an evacuated tube which extended down into the 2" electromagnet. Conduction was used for heat transfer in the cryostat. The samples were soldered onto a 5 mil thick copper sheet perpendicular to the beam with the silver eutectic solder for the Si sample and with indium solder for the Ge sample. Conductivity and Hall coefficient of those two samples were measured as the dose was increased. A series of isothermal annealing experiments from -146° to 25°C was carried out shortly after the last bombardment.

**Constructed by Superior Air Products Co., Newark, N. J.

C. CARRIER CONCENTRATION AND CONDUCTIVITY FOR SILICON IRRADIATED AT 25°C

p-type 10 Ω-cm Silicon Nominal 10 Ω-cm p-type silicon doped with boron was bombarded with electrons at energies from 12 to 40 Mev. The defect introduction rate in this energy range (measured by carrier removal), as shown in Fig. 1 appears not to depend strongly on the electron energy. A more quantitative interpretation of the data is made uncertain because the sample irradiated at 25 Mev has approximately one half the resistivity of the samples irradiated at 12 and 40 Mev. This is no doubt the reason for the apparently higher removal rate at 25 Mev. Inspection of the conductivity vs. flux curves in Fig. 2 shows a linear decrease in conductivity with flux, indicating that the Fermi level moved very little during the irradiation.

n-type 10 Ω-cm Silicon The carrier removal rate in phosphorus-doped 10 Ω cm n-type silicon showed a definite energy dependence. The three samples shown in Fig. 1 irradiated at 12, 25, and 36 Mev, indicated an increase in defect production rate as the electron energy was increased. The decrease in conductivity was quite linear over the flux range used, indicating that the Fermi level did not change significantly during the irradiation. The investigation of what levels are being introduced will be carried out by a study of the temperature dependence of the carrier concentration.

A comparison in Fig. 1 of the damage produced in 10 Ω-cm p-type and n-type Si shows a definitely lower damage rate for the p-type material at all energies investigated.

A further comparison of the measured carrier removal rates for nominal 10 Ω-cm n-type germanium and silicon is tabulated below. The values are taken by interpolation from the curves of Fig. 1 and similar data for germanium to be presented below.

Energy (Mev)	Measured Carrier Removal Rate (carriers/electron-cm)	
	Ge	Si
10	1.3	.23
25	1.2	.38
40	1.4	.50

At the higher energies, the carrier removal rate for germanium is measured to be approximately three times that of silicon. The Mott-McKinley-Feshbach cross-section formula used with the Kinchin-Pease model indicates that for a displacement threshhold of 15 ev, the ratio of germanium damage to silicon damage should be slightly less than two. The measured values do, however, agree at least qualitatively with the theory.

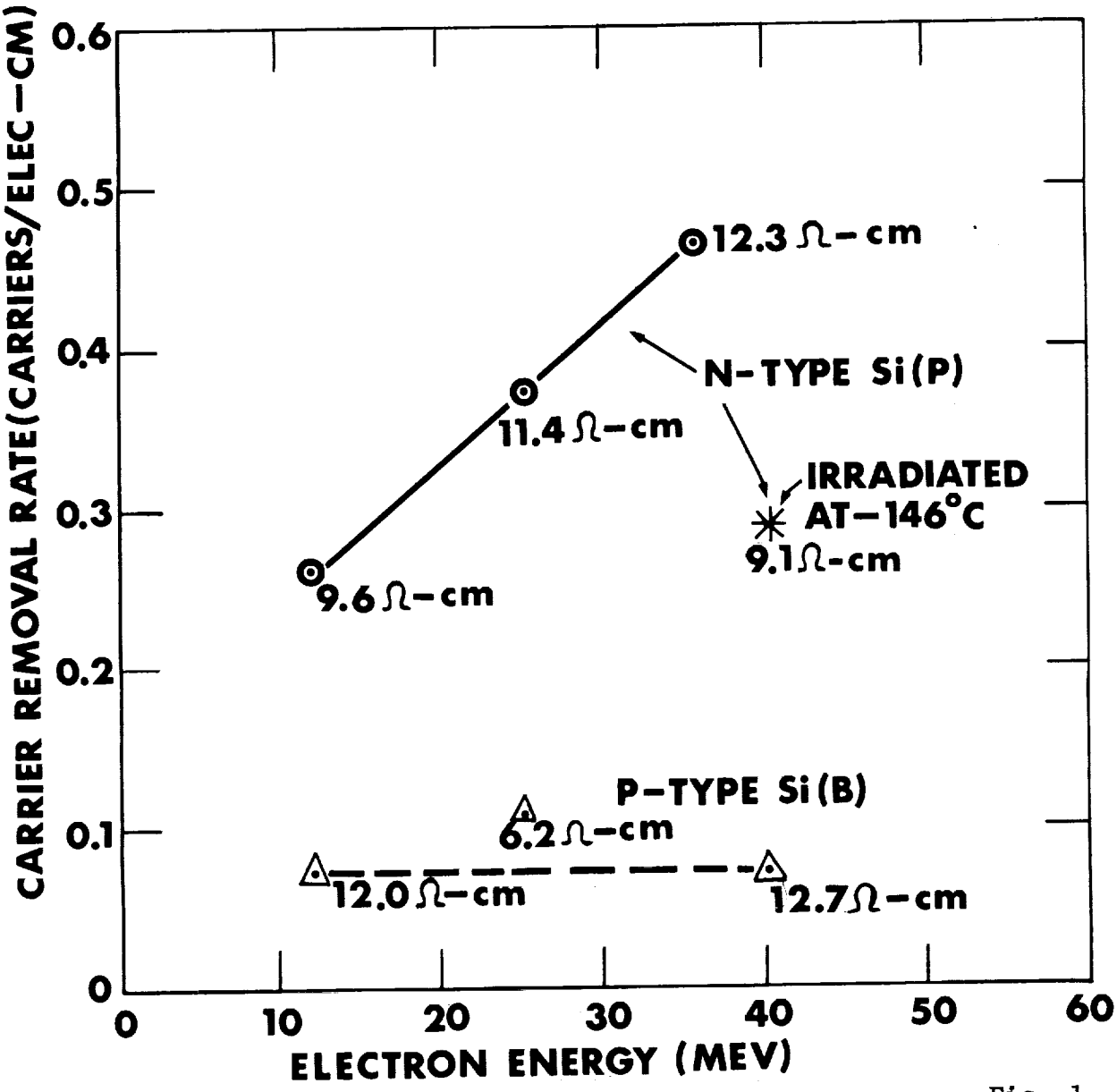
CARRIER REMOVAL RATE(CARRIERS/ELEC-CM)
0.6
0.5
0.4
0.3
0.2
0.1
0
0
10
20
30
40
50
60
ELECTRON ENERGY (MEV)
12.3 Ω-cm
N-TYPE Si(P)
11.4 Ω-cm
IRRADIATED
AT-146°C
9.1Ω-cm
9.6 Ω-cm
P-TYPE Si(B)
6.2 Ω-cm
12.0 Ω-cm
12.7Ω-cm

Fig. 1

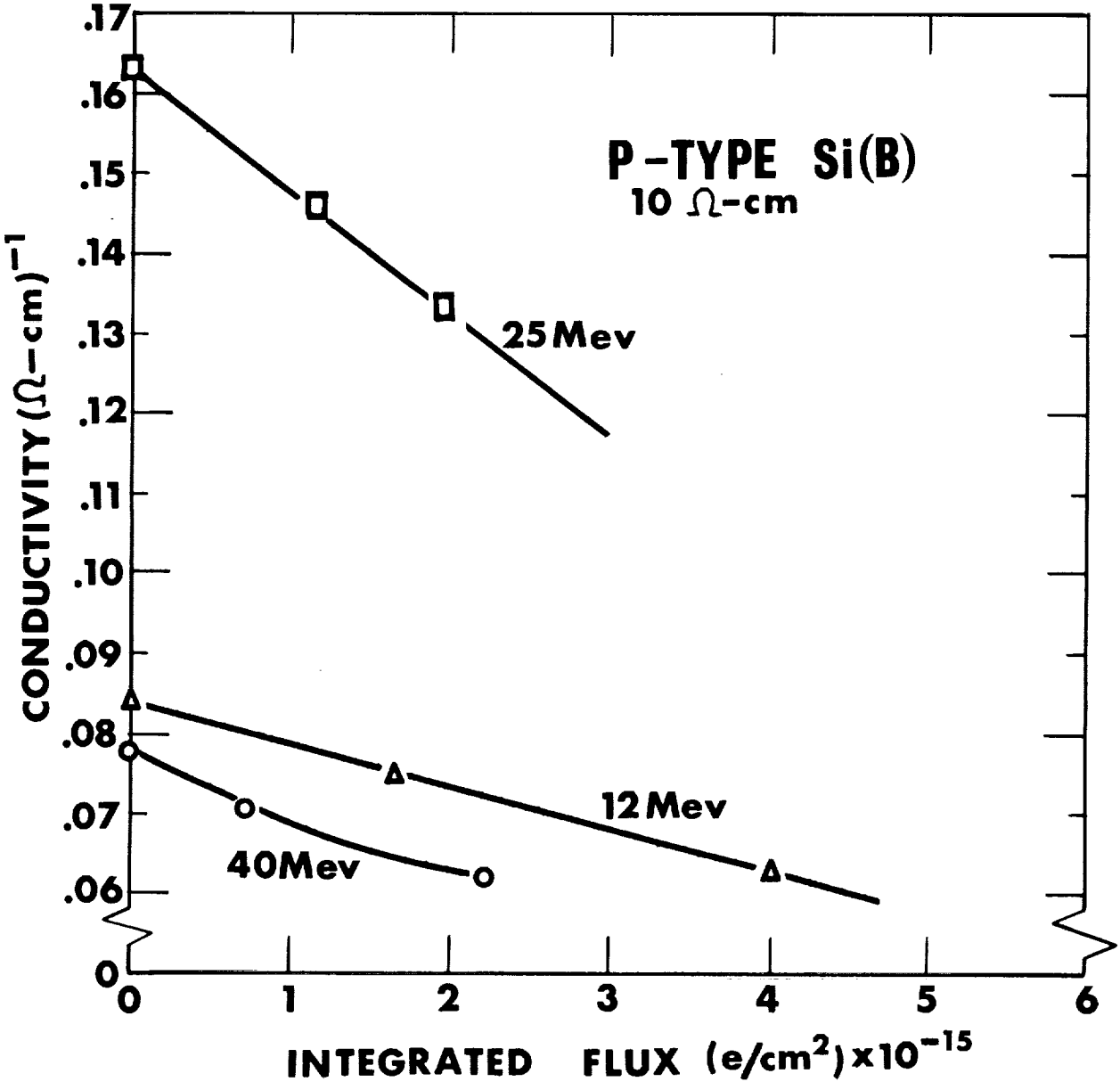
P-TYPE Si(B)
10 Ω-cm
25 Mev
12 Mev
40 Mev
CONDUCTIVITY (Ω-cm)⁻¹
.17
.16
.15
.14
.13
.12
.11
.10
.09
.08
.07
.06
0
0
1
2
3
4
5
6
INTEGRATED FLUX (e/cm²) x10⁻¹⁵

Fig. 2

n-Type Silicon 1 Ω-cm The 1 Ω-cm phosphorus-doped n-type silicon was irradiated at 17 Mev and 35 Mev. Carriers were removed at a greater rate by the lower energy electrons, as shown in Fig. 3. The conductivity change shown in Fig. 4 was nearly the same for both energies. This behavior, which is anomalous in light of the present understanding of energy dependence, cannot be explained by a difference in initial characteristics of the two samples, as the original Hall coefficients and conductivities were very nearly the same. Furthermore, errors in flux measurements were not large enough to explain the results. Since only two samples were irradiated, further conclusions will have to await future detailed experiments.

D. CARRIER CONCENTRATION AND CONDUCTIVITY FOR GERMANIUM IRRADIATED AT 25°C

n-Type Germanium 10 Ω-cm Antimony Doped Figures 5, 6, and 7 show the conductivity, carrier concentration and Hall mobility respectively for samples bombarded at energies of 12, 25, and 54 Mev. While the conductivity and carrier concentration appear to be changing at approximately the same rate for the 12 and 25 Mev samples, the 54 Mev sample shows a definite increase in the rate of change of these properties. Figure 7 shows that the Hall mobility undergoes only a small decrease for the 12 and 25 Mev samples, while the 54 Mev sample shows a 15% decrease.

n-Type Germanium 20 Ω-cm Antimony Doped In Figures 8, 9, and 10 we show the electrical properties as a function of integrated electron flux for various electron energies in the range 12 to 54 Mev. At low fluxes it is seen that the rate of change in conductivity increases with an increase in energy. The rate of change of the carrier concentration for the 12 Mev sample and the 25 Mev sample appears to be about the same. We do observe however an increase in the rate of change of carrier concentration for the 54 Mev sample. Figure 10 shows that the Hall mobility for the 12 and 54 Mev samples decreases at the same rate for fluxes between 1×10^{13} electrons/cm^2 and 3×10^{13} electrons/cm^2.

n-Type Germanium 35 Ω-cm Arsenic Doped Figure 11 shows the conductivity and Hall coefficient of high purity germanium which changed from n-type to p-type during the irradiation. Since the material is near intrinsic to start with the two band theory will be necessary to explain the data. According to the two band theory the conductivity and Hall coefficient are given by

$$\sigma = n_e e \mu_e + n_h e \mu_h$$

$$R_H = \frac{3\pi}{8ec} \frac{(n_h \mu_h^2 - n_e \mu_e^2)}{(n_h \mu_h + n_e \mu_e)^2}$$

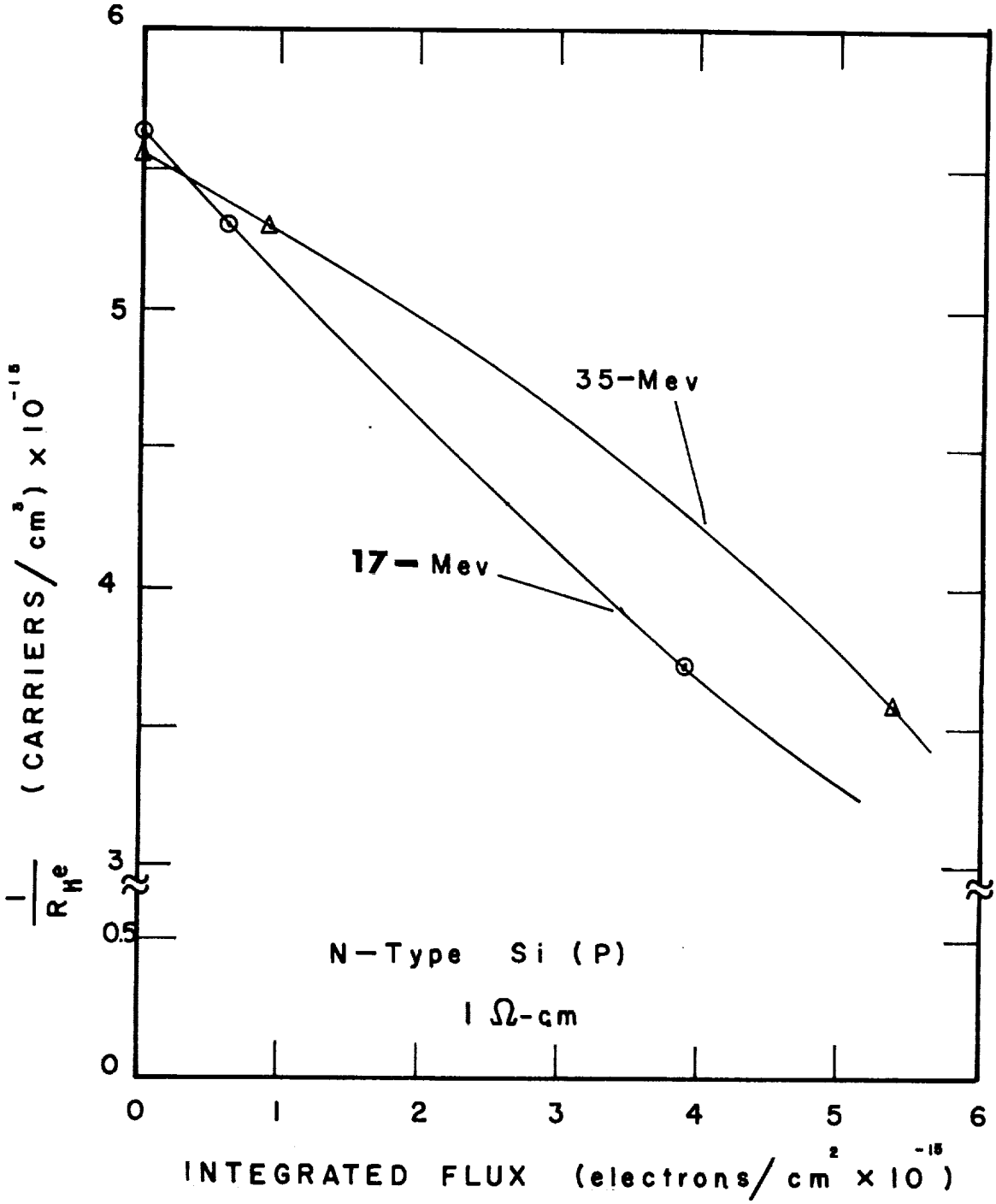
6
5
4
3
0.5
0
0
1
2
3
4
5
6
35-Mev
17-Mev
N-Type Si (P)
1 Ω-cm
$\frac{1}{R_H e}$ (CARRIERS/cm^3) x 10^{-15}
INTEGRATED FLUX (electrons/cm^2 x 10^{-15})

Fig. 3

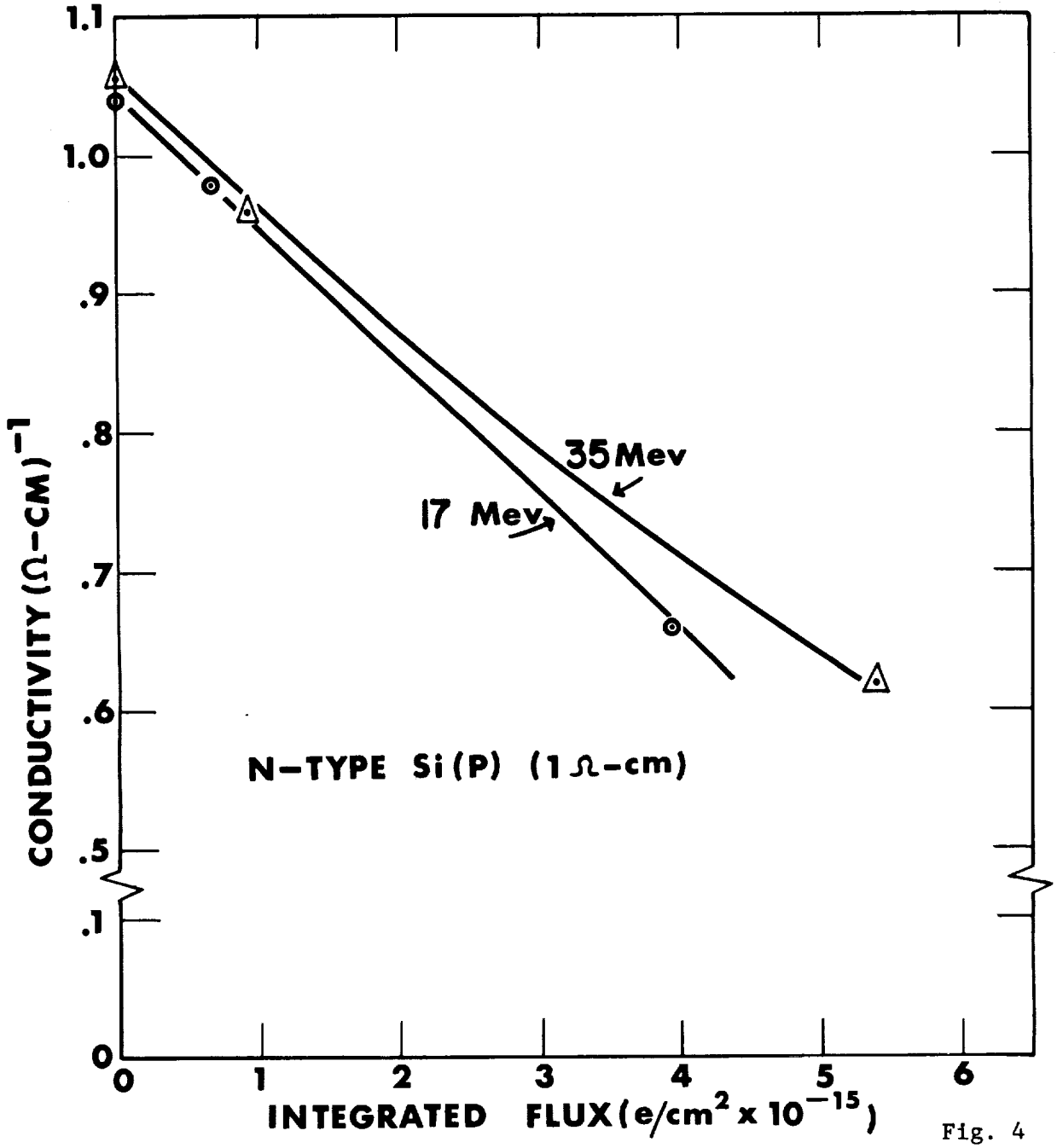
1.1
1.0
.9
.8
.7
.6
.5
.1
0
0
1
2
3
4
5
6
CONDUCTIVITY (Ω-CM)$^{-1}$
INTEGRATED FLUX (e/cm^2 x 10^{-15})
35 Mev
17 Mev
N-TYPE Si (P) (1 Ω-cm)

Fig. 4

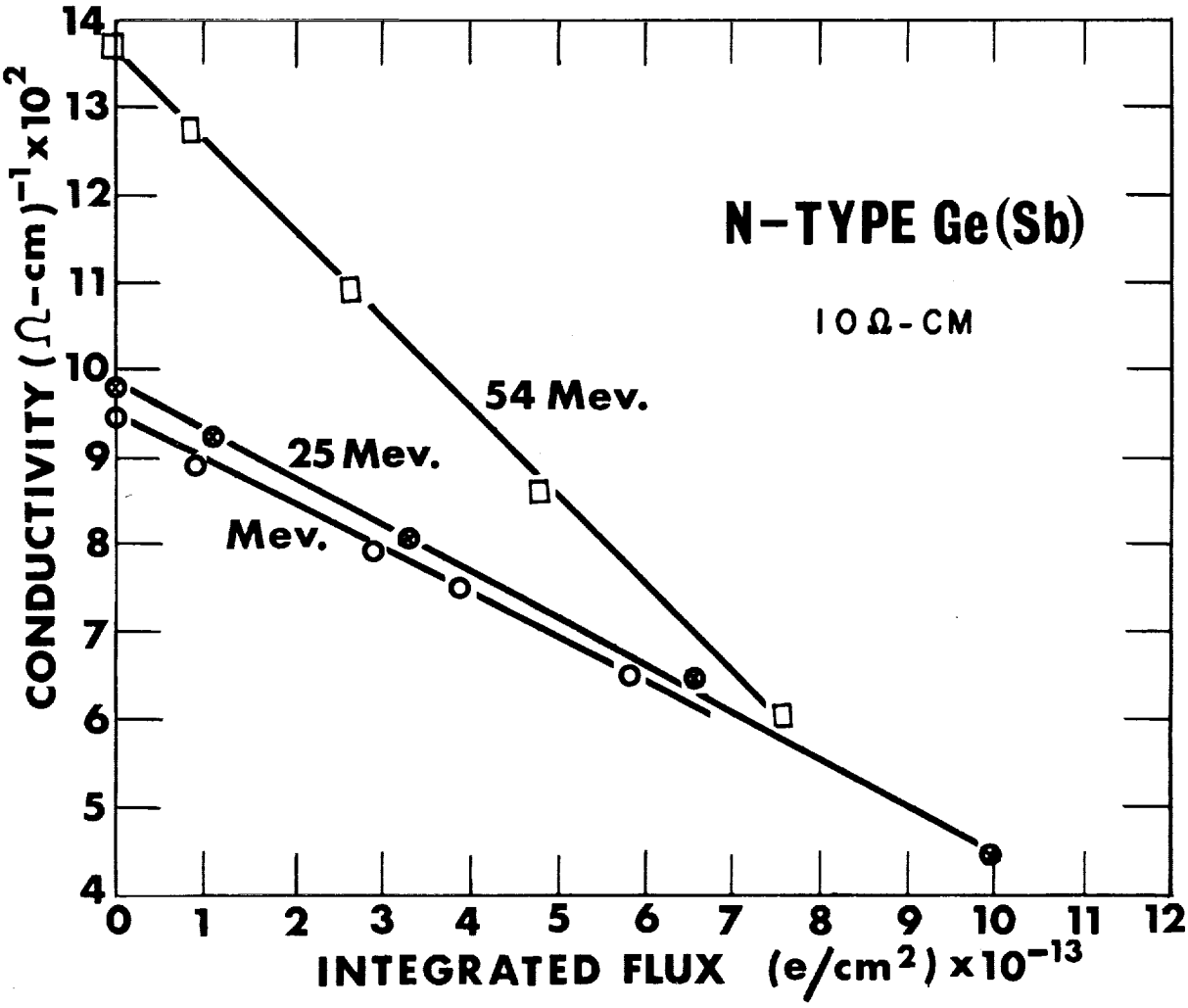
N-TYPE Ge(Sb)
10 Ω-CM
54 Mev.
25 Mev.
Mev.
CONDUCTIVITY $(\Omega\text{-cm})^{-1} \times 10^{2}$
INTEGRATED FLUX $(e/cm^2) \times 10^{-13}$
14
13
12
11
10
9
8
7
6
5
4
0
1
2
3
4
5
6
7
8
9
10
11
12

Fig. 5

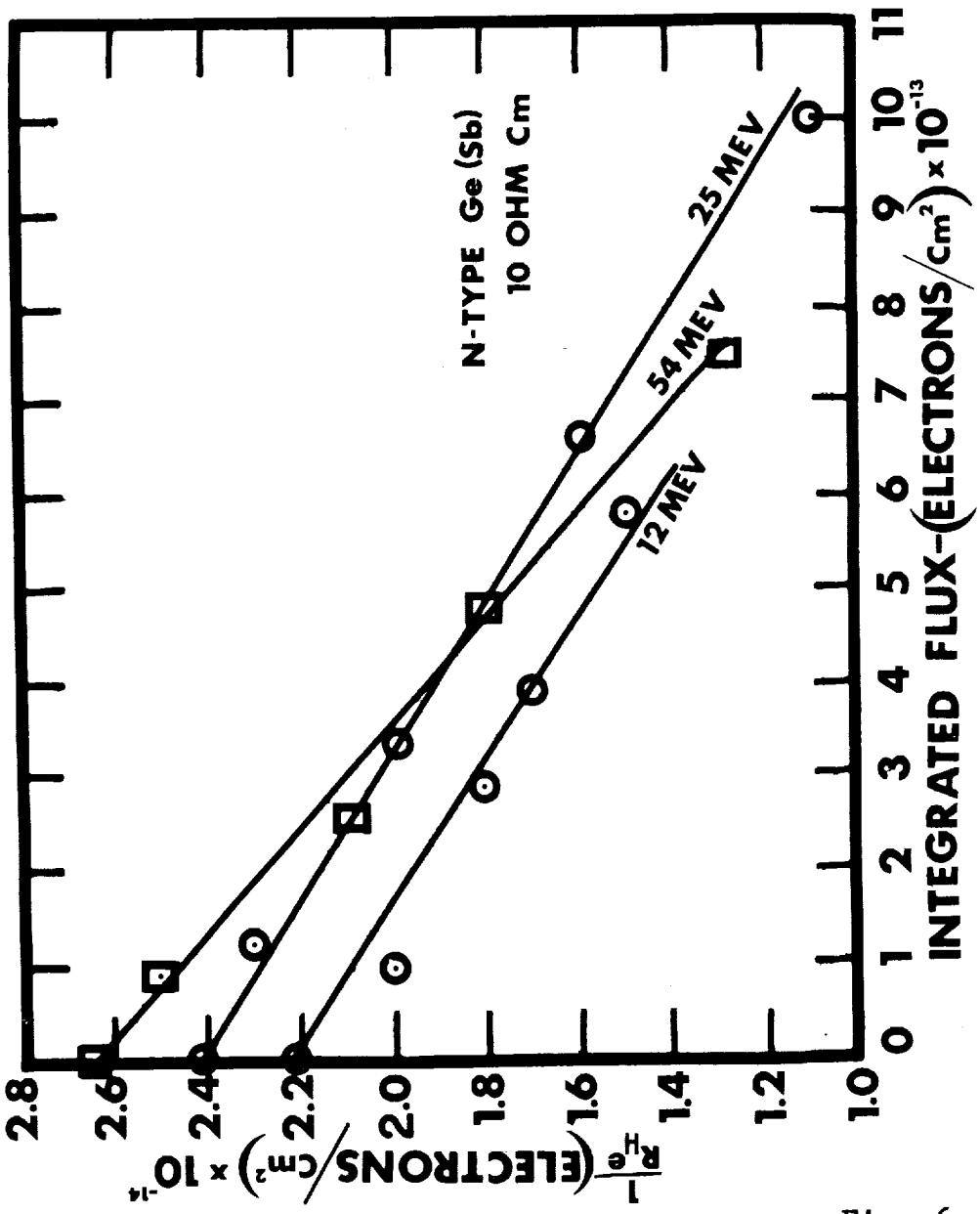
N-TYPE Ge (Sb)
10 OHM Cm
25 MEV
54 MEV
12 MEV
INTEGRATED FLUX-(ELECTRONS/Cm²) x 10⁻¹³
1/R_He (ELECTRONS/Cm³) x 10⁻¹⁴
0
1
2
3
4
5
6
7
8
9
10
11
1.0
1.2
1.4
1.6
1.8
2.0
2.2
2.4
2.6
2.8

Fig. 6

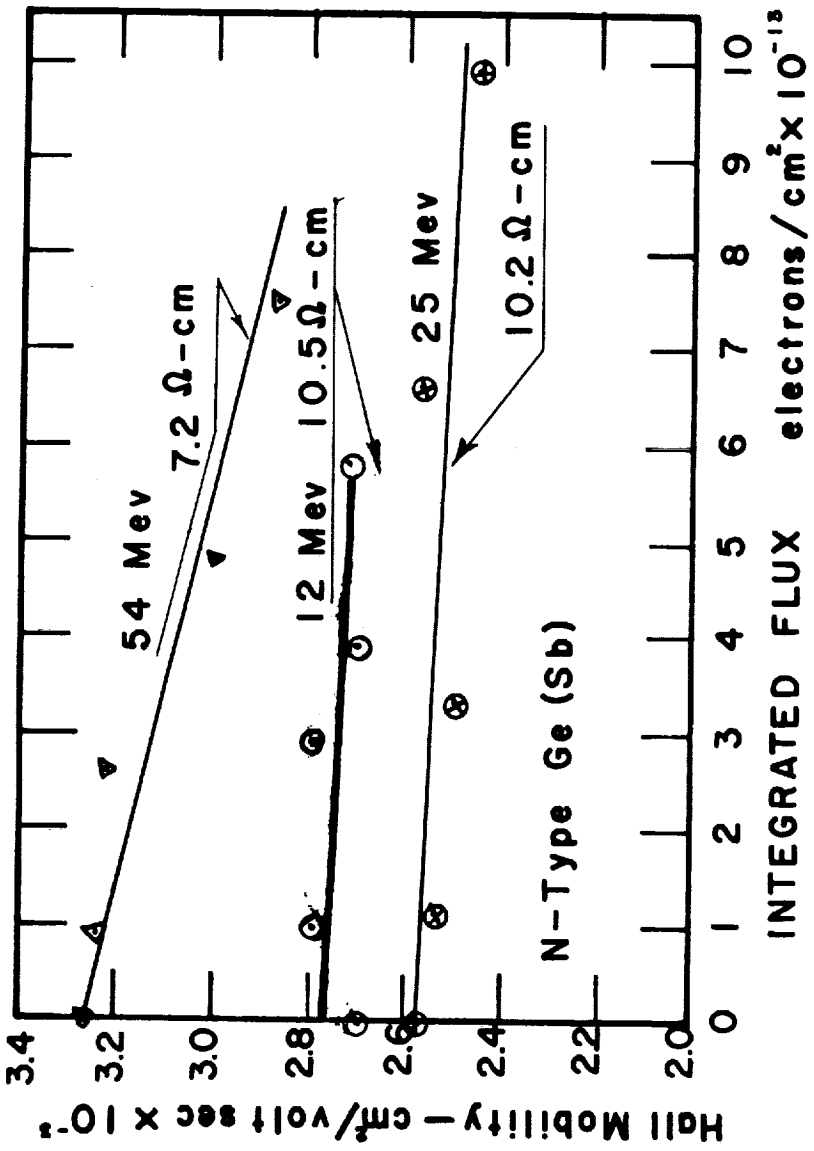
Hall Mobility — cm²/volt sec x 10⁻⁴
3.4
3.2
3.0
2.8
2.6
2.4
2.2
2.0
0 1 2 3 4 5 6 7 8 9 10
INTEGRATED FLUX electrons/cm² x 10⁻¹⁵
N-Type Ge (Sb)
54 Mev
7.2 Ω-cm
12 Mev
10.5Ω-cm
25 Mev
10.2 Ω-cm

Fig. 7

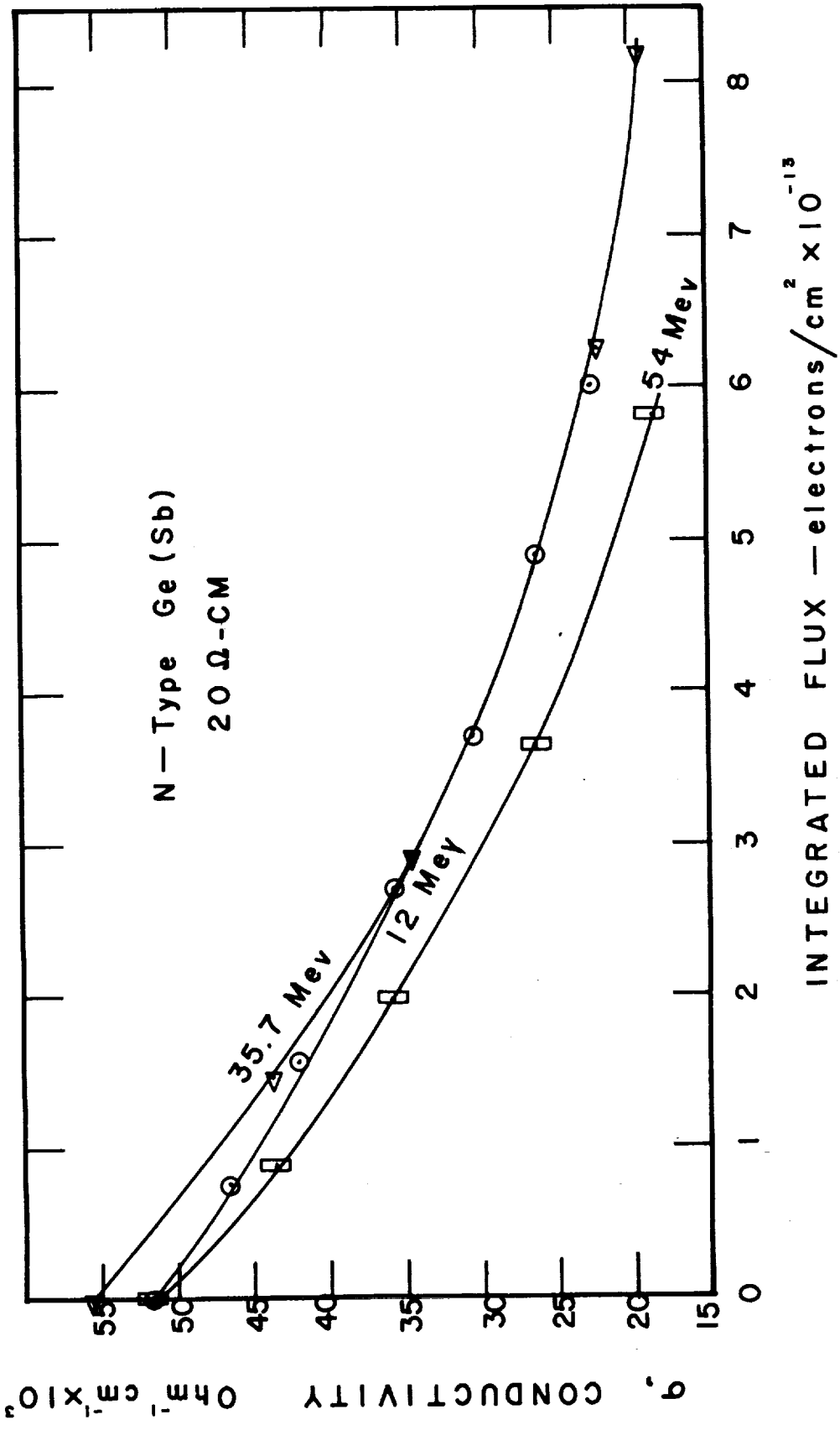
N — Type Ge (Sb)
20 Ω-CM
35.7 Mev
12 Mev
54 Mev
INTEGRATED FLUX — electrons/cm² x 10⁻¹³
q, CONDUCTIVITY ohm⁻¹ cm⁻¹ x 10³

Fig. 8

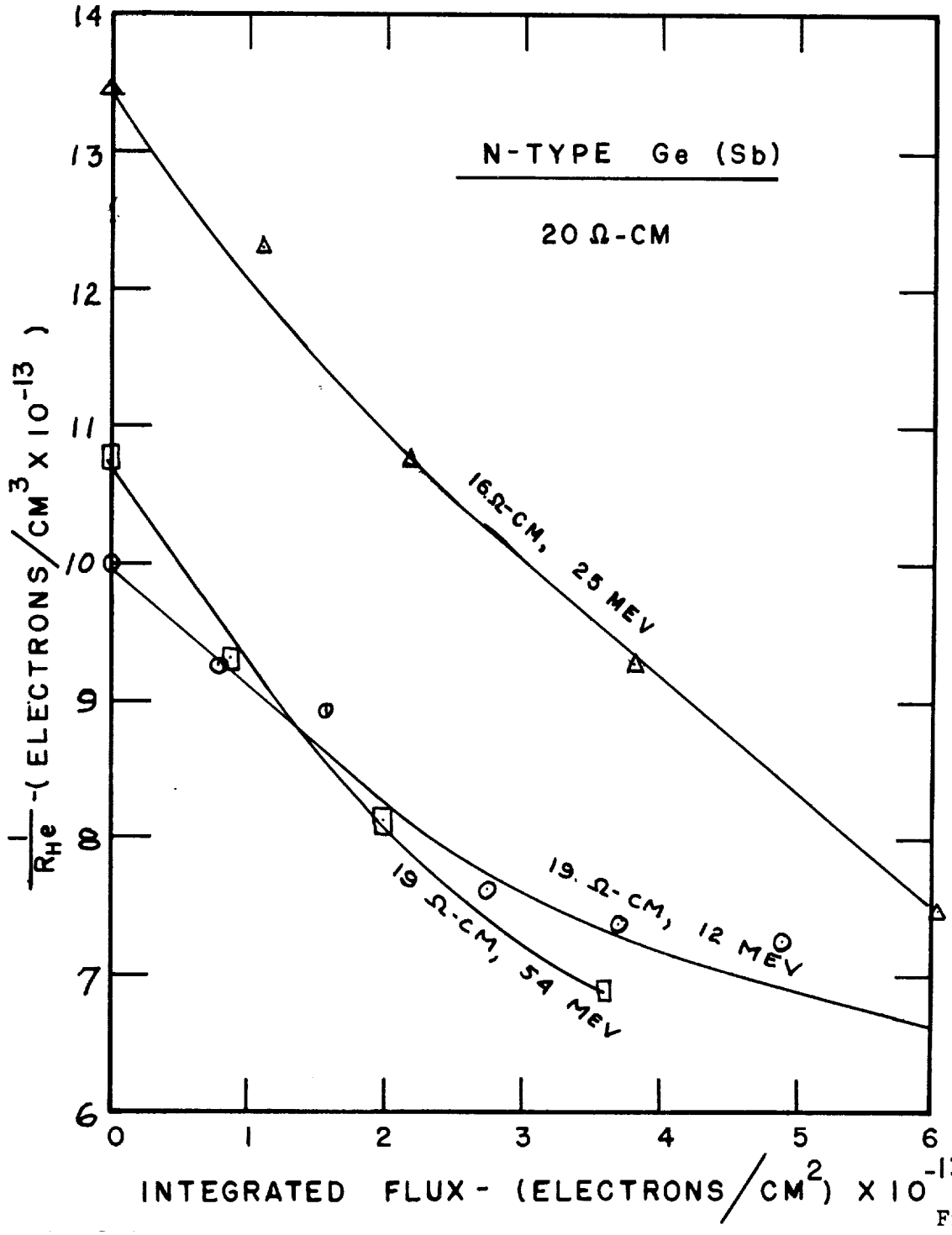
N-TYPE Ge (Sb)
20 Ω-CM
16 Ω-CM, 25 MEV
19 Ω-CM, 12 MEV
19 Ω-CM, 54 MEV
$\frac{1}{R_H e}$ - (ELECTRONS/CM^3 X 10^{-13})
INTEGRATED FLUX - (ELECTRONS/CM^2) X 10^{-13}
14
13
12
11
10
9
8
7
6
0
1
2
3
4
5
6

Fig. 9

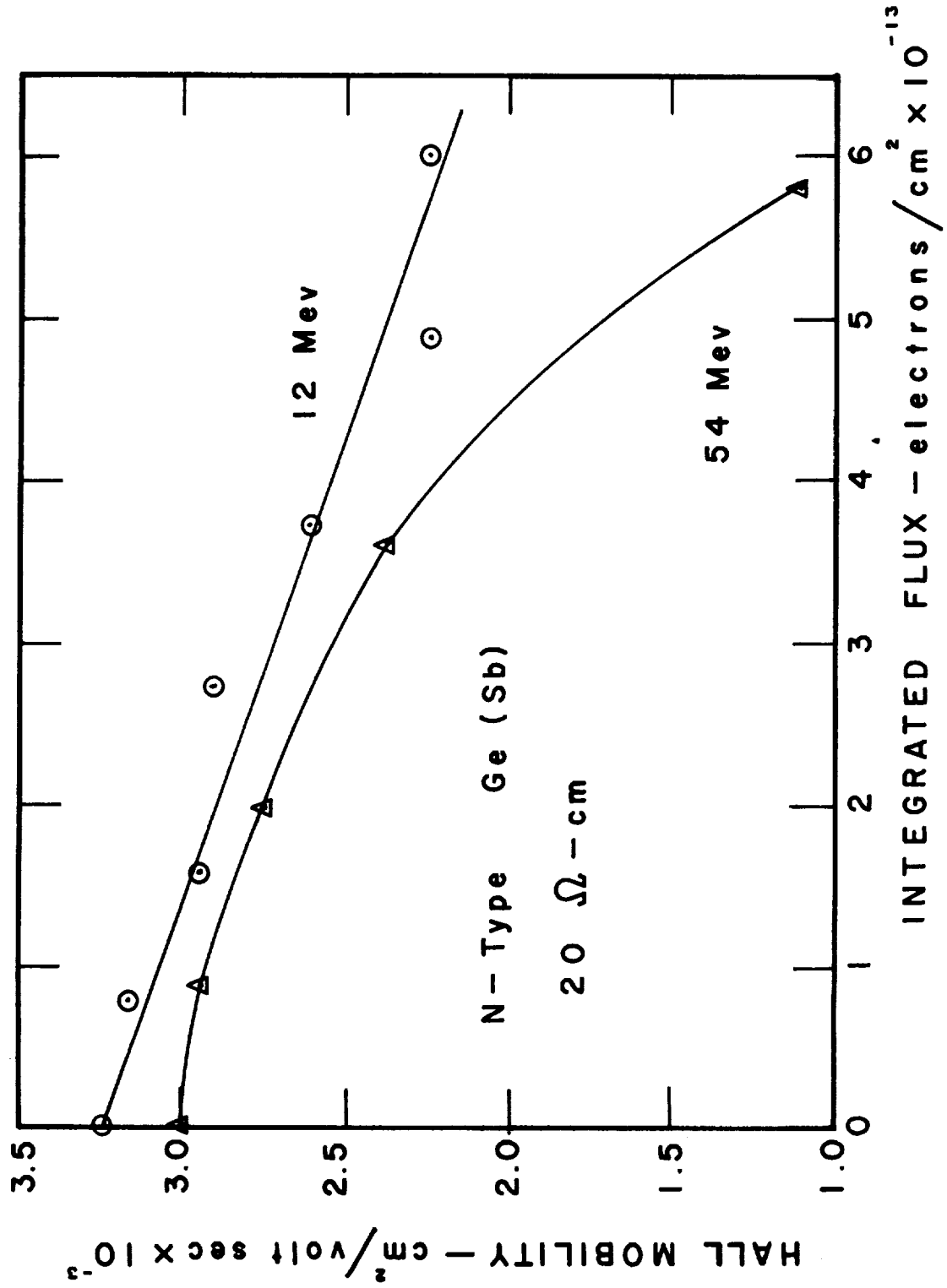
HALL MOBILITY — cm²/volt sec x 10⁻³
INTEGRATED FLUX — electrons/cm² x 10⁻¹³
12 Mev
54 Mev
N — Type Ge (Sb)
20 Ω — cm
3.5
3.0
2.5
2.0
1.5
1.0
0
1
2
3
4
5
6

Fig. 10

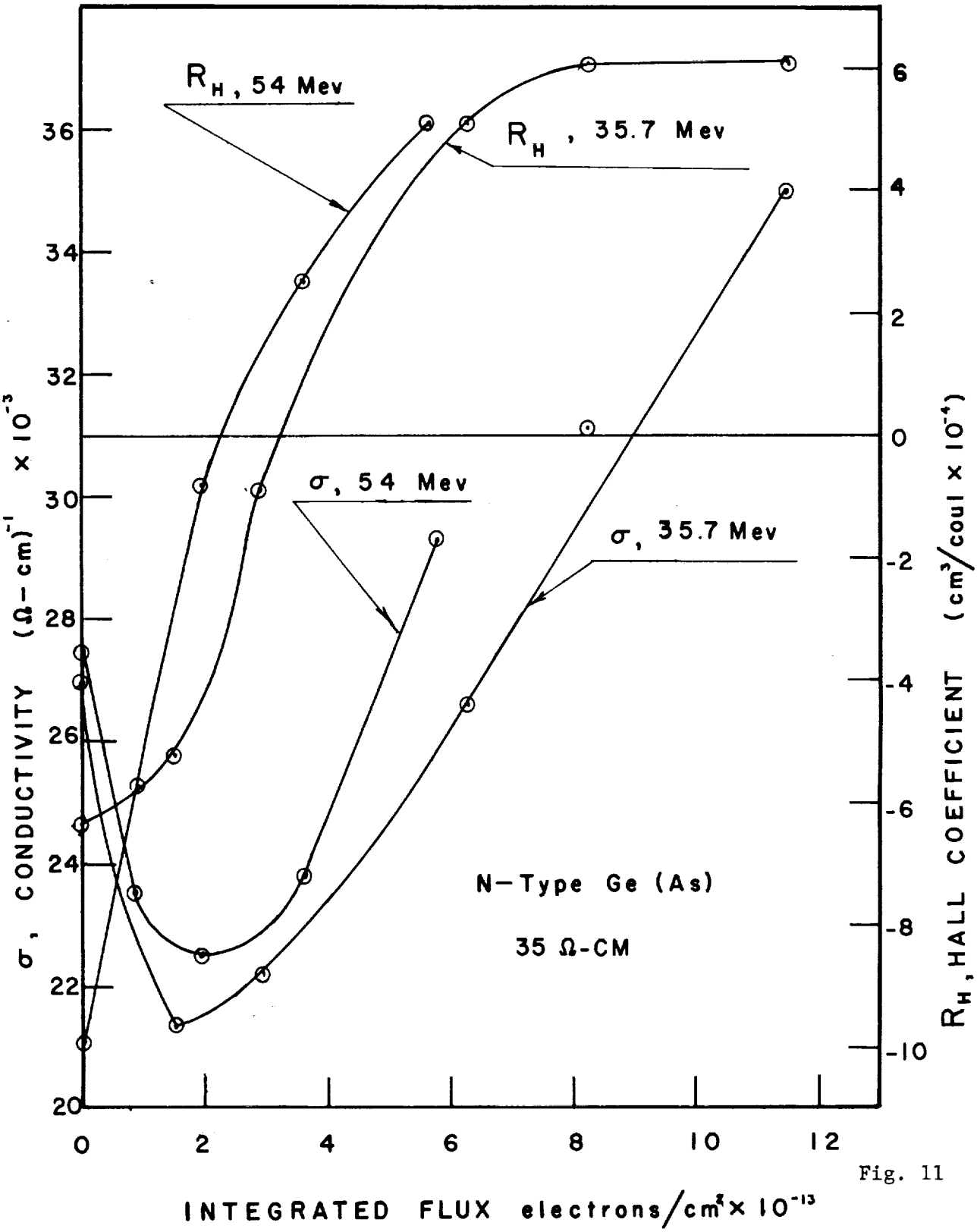
R_H, 54 Mev
R_H, 35.7 Mev
σ, 54 Mev
σ, 35.7 Mev
N-Type Ge (As)
35 Ω-CM
σ, CONDUCTIVITY (Ω-cm)$^{-1}$ × 10^{-3}
R_H, HALL COEFFICIENT (cm^3/coul × 10^{-4})
INTEGRATED FLUX electrons/cm^2 × 10^{-13}
36
34
32
30
28
26
24
22
20
6
4
2
0
-2
-4
-6
-8
-10
0
2
4
6
8
10
12

Fig. 11

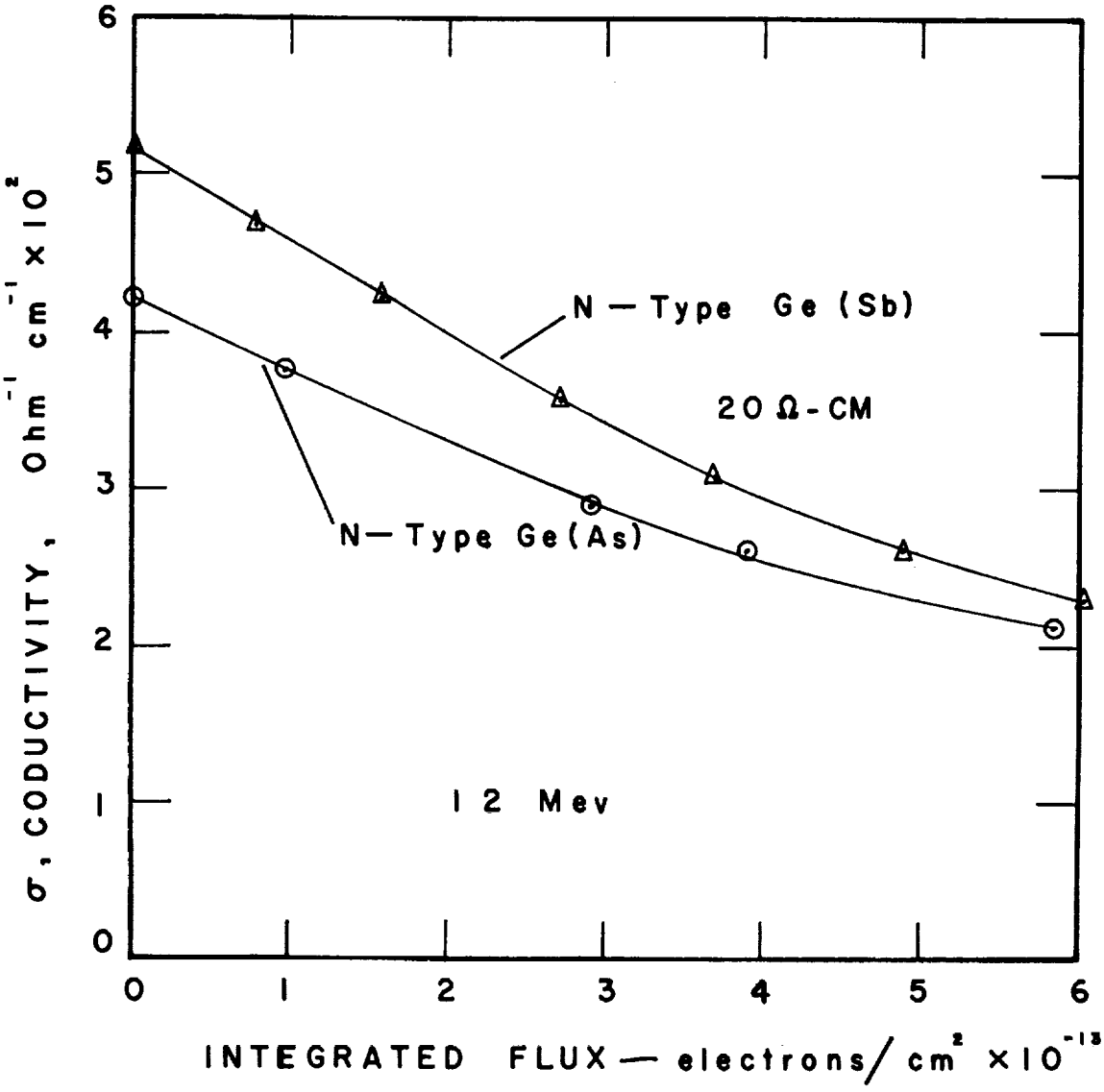
σ, CODUCTIVITY, Ohm⁻¹ cm⁻¹ x 10²
N — Type Ge (Sb)
20 Ω-CM
N— Type Ge(As)
1 2 Mev
INTEGRATED FLUX — electrons/ cm² x 10⁻¹³
0
1
2
3
4
5
6

Fig. 12

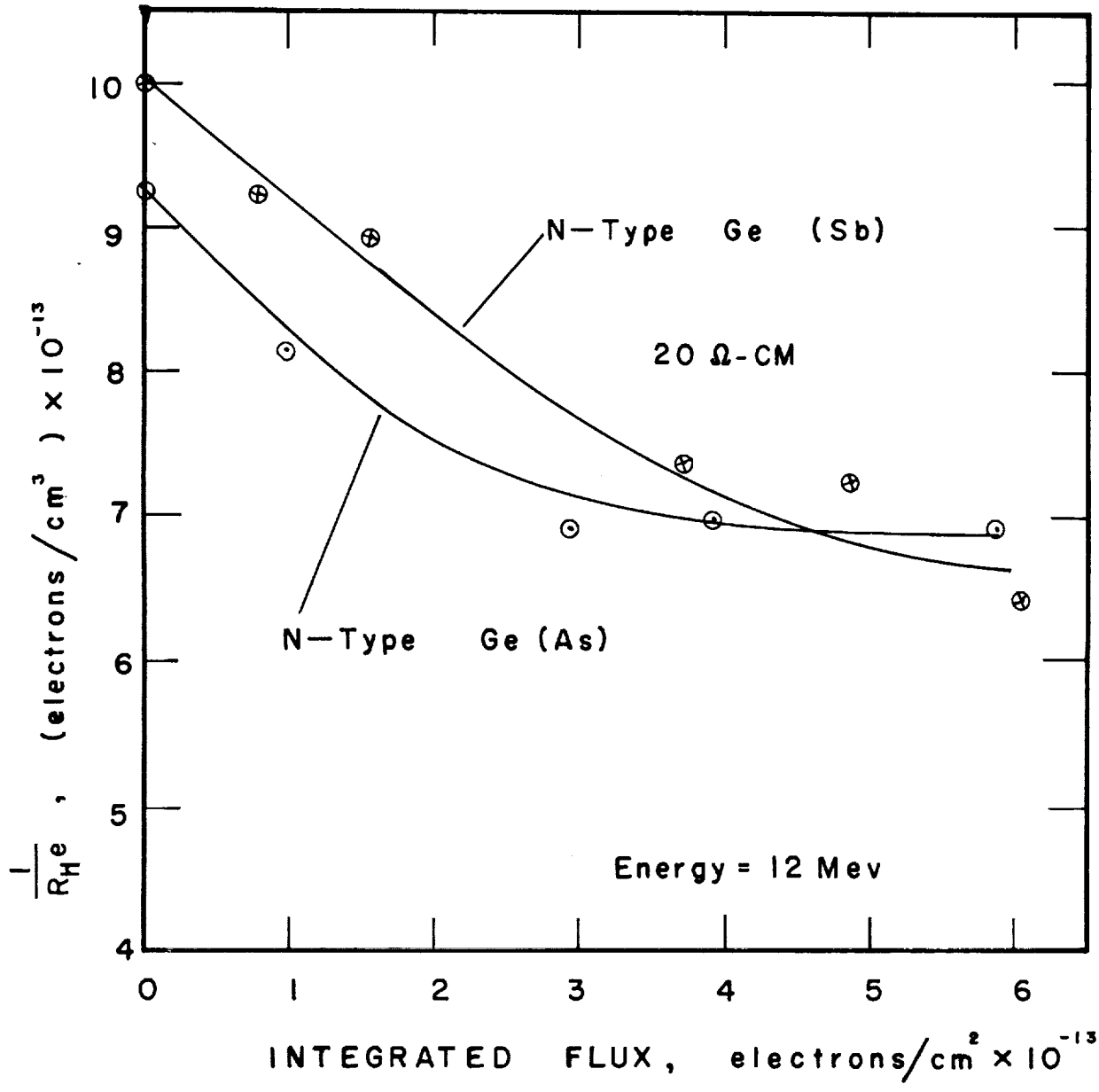
N—Type Ge (Sb)
20 Ω-CM
N—Type Ge (As)
Energy = 12 Mev
$\frac{1}{R_H e}$, (electrons/cm^3) x 10^{-13}
INTEGRATED FLUX, electrons/cm^2 x 10^{-13}
10
9
8
7
6
5
4
0
1
2
3
4
5
6

Fig. 13

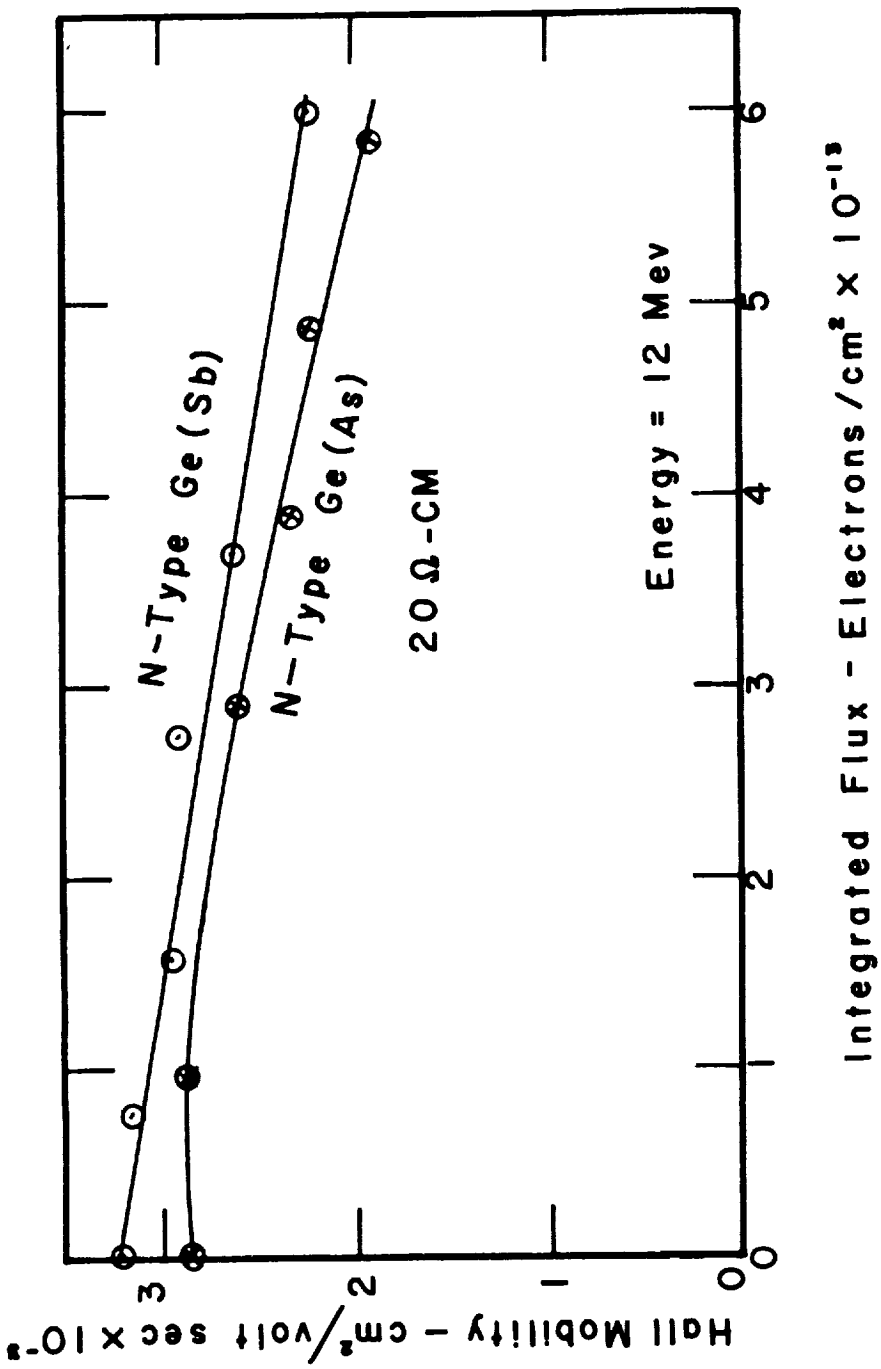
Hall Mobility – cm²/volt sec x 10⁻³
0
1
2
3
Integrated Flux - Electrons/cm² x 10⁻¹³
0
1
2
3
4
5
6
Energy = 12 Mev
20 Ω-CM
N-Type Ge (As)
N-Type Ge (Sb)

Fig. 14

where e and h refer to electrons and holes. Under increased irradiation the value of n_h increases while n_e decreases. Beyond this point the $n_h e\mu_h$ term dominates and the conductivity increases. At the beginning $n_e\mu_e^2$ is greater than $n_h\mu_h^2$. As the irradiation continues a condition is reached where $n_h\mu_n^2$ equals $n_e\mu_e^2$ and the Hall coefficient becomes zero. Beyond this $n_h\mu_h^2$ becomes the dominant term in the numerator and the Hall coefficient increases positively. For low fluxes the conductivity appears to be energy independent while Hall coefficient increases more rapidly for the 54 Mev sample than for the 35.7 Mev sample.

Effect of Arsenic and Antimony doping in n-type Germanium 20 Ω -cm Irradiated with 12 Mev Electrons Figures 12, 13 and 14 show the effect of doping on the change in electrical properties. The samples studied were irradiated at 12 Mev. In figure 12 we observe that the antimony doped sample appears to have its conductivity change faster than the arsenic doped sample. It should be pointed out however that the antimony doped sample has a higher initial conductivity and would be expected to have its conductivity change faster for this reason alone.

At lower fluxes the rate of change of carrier concentration appears to be about the same for both samples. Figure 14 shows that the Hall mobility of both samples changes at the same rate in the middle of the flux range studied. At fluxes less than 1×10^{13} $\frac{\text{electrons}}{\text{cm}^2}$ the Hall mobility of the arsenic doped sample remains constant. In general we conclude that within experimental error the rate of damage appears to be independent of the two types of doping (Sb and As) studied in this experiment.

p-type Germanium 10 Ω cm Indium Doped Figures 15 and 16 show the electrical properties for p-type germanium bombarded by electrons of various energies in the range 12 to 40 Mev. The conductivity data of Fig. 15 indicates a small dependence of conductivity change on electron energy. The rate of addition of carriers (holes) Fig. 16 shows a more pronounced dependence on energy, and the addition rate increases with energy.

Carrier Removal Rates as Function of Energy In Figure 17 we show the carrier removal rates for n- and p-type germanium. In order to compare the theory with experiment it will be necessary to compare these values with the number of atoms removed from their lattice sites as predicted by theory. In keeping with the notation of Simon, Denney and Downing[6] we define a defect density which is equal to the number of atoms displaced for an incident flux of one particle per cm^2. This gives the total number of lattice displacements per cm. To obtain this value we use the Mott-McKinley-Feshbach[7] relativistic electron cross section and the Kinchin and Pease[7] model for g(T), where g(T) represents the number of displacements per primary knock on of energy T.

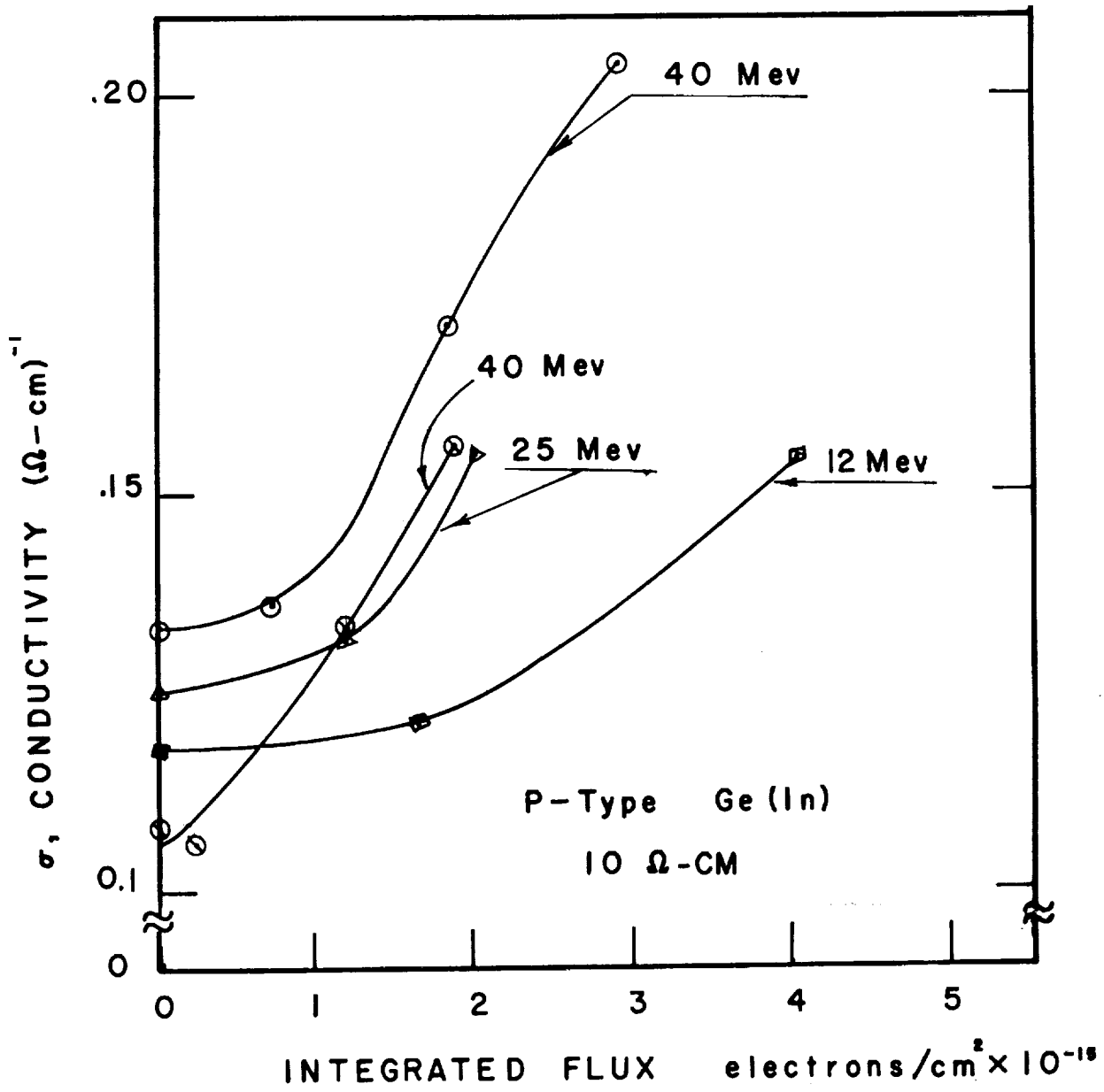
40 Mev
40 Mev
25 Mev
12 Mev
P-Type Ge (In)
10 Ω-CM
.20
.15
0.1
0
σ, CONDUCTIVITY (Ω-cm)⁻¹
0
1
2
3
4
5
INTEGRATED FLUX electrons/cm² × 10⁻¹⁵

Fig. 15

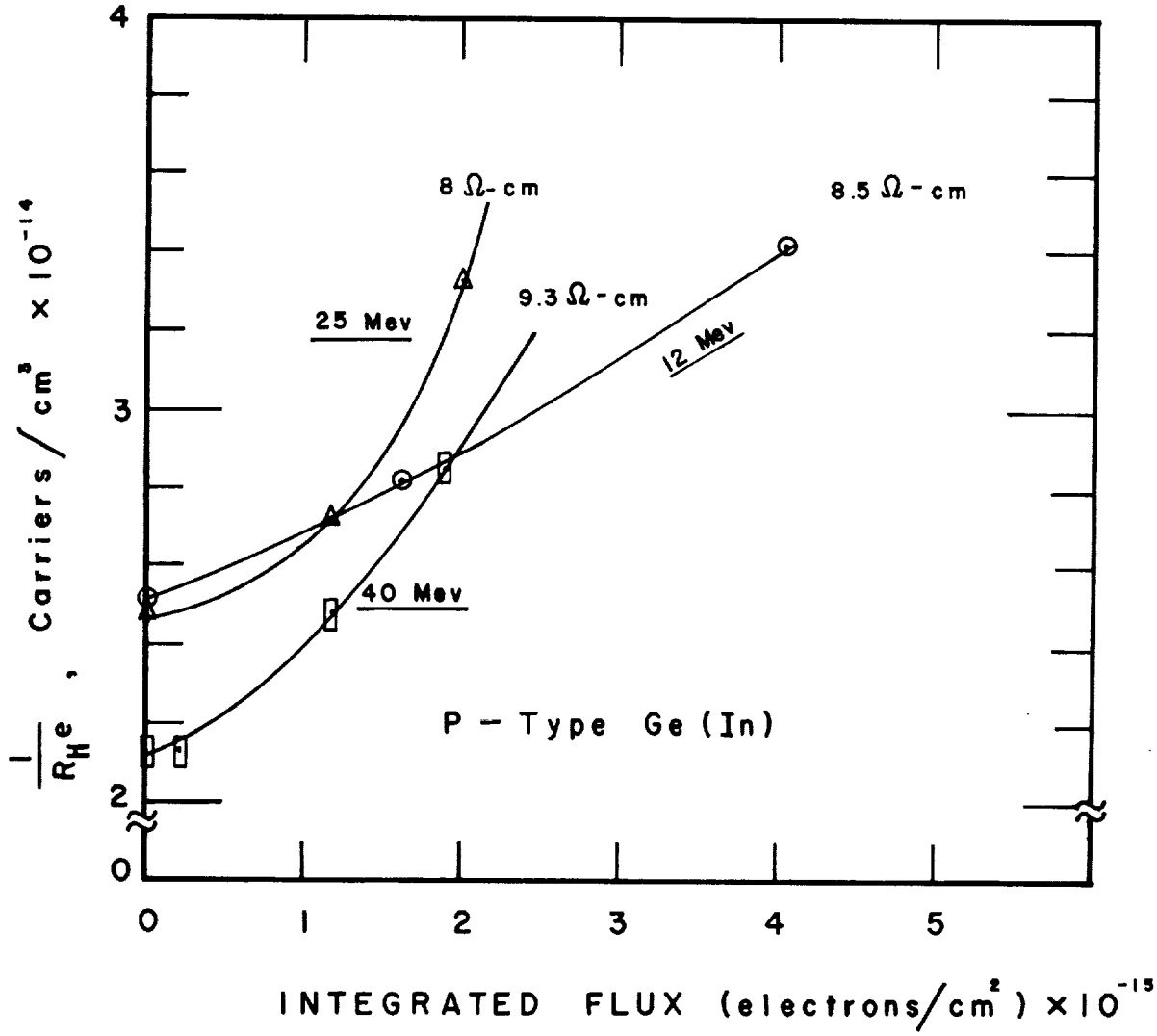
4
3
2
0
0
1
2
3
4
5
8 Ω-cm
8.5 Ω-cm
9.3 Ω-cm
25 Mev
12 Mev
40 Mev
P – Type Ge (In)
$\frac{1}{R_H e}$, Carriers / cm³ × 10⁻¹⁴
INTEGRATED FLUX (electrons/cm²) × 10⁻¹⁵

Fig. 16

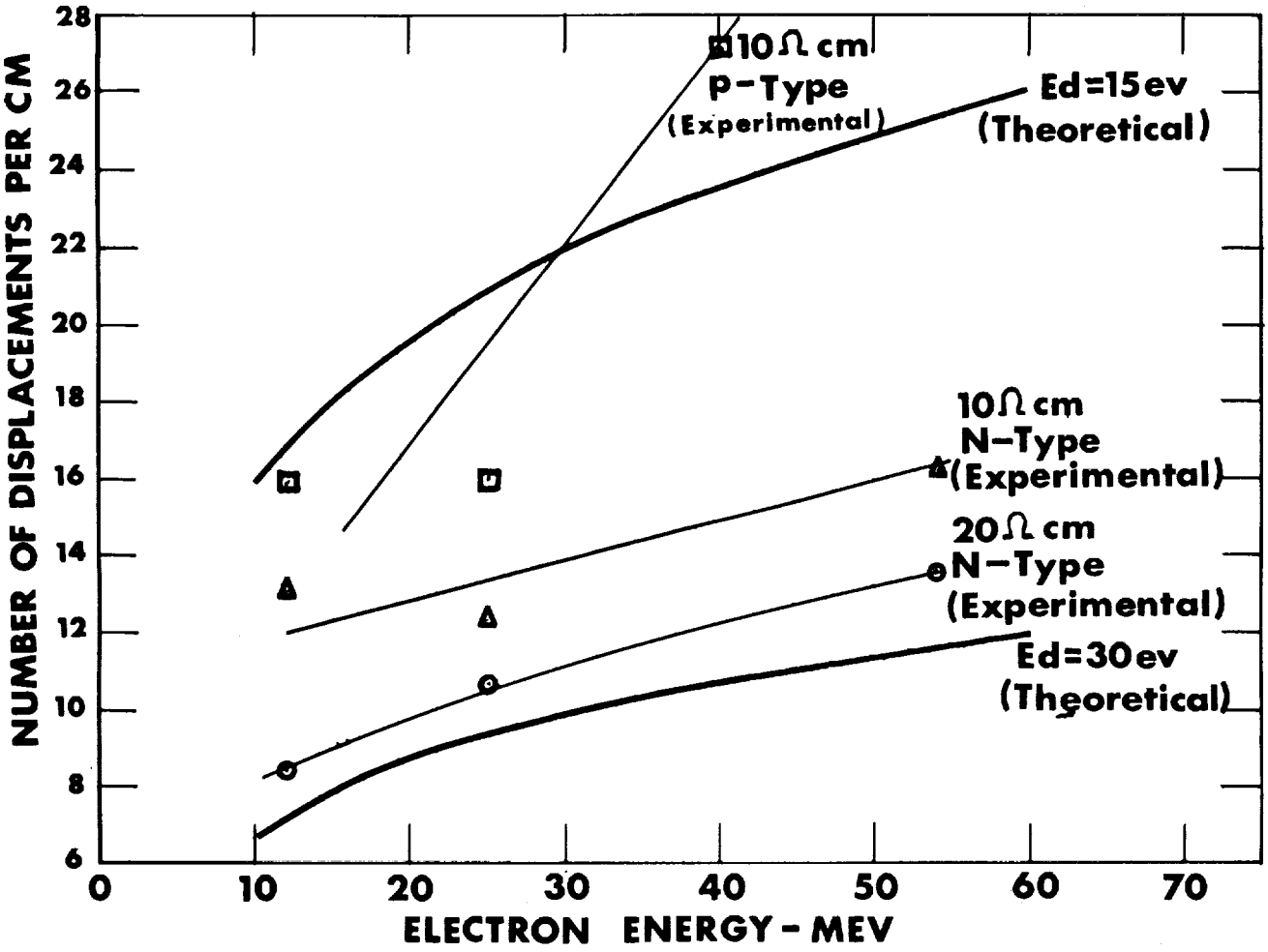
NUMBER OF DISPLACEMENTS PER CM
ELECTRON ENERGY - MEV
10Ω cm
P-Type
(Experimental)
Ed=15ev
(Theoretical)
10Ω cm
N-Type
(Experimental)
20Ω cm
N-Type
(Experimental)
Ed=30ev
(Theoretical)
28
26
24
22
20
18
16
14
12
10
8
6
0
10
20
30
40
50
60
70

Fig. 17

In Table I we show the calculated and measured defect production rates for germanium.

TABLE I

Electron Energy Mev	Type	Resistivity ohm cm	Defect production rate per incident electron		
			Calculated		Measured
			Ed=15ev	Ed=30ev	
12	n	19.3	16.8	9.2	.85
25	n	15.6	20.9	9.4	.86
54	n	19.3	25.4	11.8	1.36
12	n	10.5	16.8	9.2	1.31
25	n	10.2	20.9	9.4	1.24
54	n	7.2	25.4	11.8	1.63
12	p	8.5	16.8	9.2	.016
25	p	7.3	20.9	9.4	.016
40	p	9.3	23.6	10.8	.027

In Tables II and III we show calculated and measured defect production rate as reported by other experimenters.

TABLE II

Electron Energy	Calculated defects per incident electron		Measured Acceptor Centers per Incident Electron
	Ed=15ev	Ed=30ev	
1.5 Mev	0.23	0.059	0.065
1.8	0.26	0.082	0.135

TABLE III

Electron Energy	Thickness	Defect Production Rate Calculated		Measured
		Ed=15ev	Ed=30ev	
0.7 Mev	0.01 cm	2.44 cm^{-1}		0.10 cm^{-1}
1.0	0.01	3.95	0.60 cm^{-1}	1.00
2.5	0.01	10	3.4	3.9
4.5	0.03	11.3	4.5	4.8
5.0	0.03	12.0	5.0	5.0

Table II shows the results of Klontz taken at liquid nitrogen, while Table III shows the results of Klontz taken at room temperature and analyzed in Cahn's paper.[8]

In analyzing the data it should be kept in mind that the theory does not account for room temperature annealing or the type of doping. The experimental data will be in error due to uncertainties in flux measurements. Thus we use as an index of the relationship between theory and experiment the shape of the experimental and theoretical curves rather than absolute values.

Let us define a quantity which for convenience we shall call the ratio of the defect density at the end point energies (ROD). For the n-type Ge we use end point values for 12 and 54 Mev. For the p-type Ge we use values for 12 and 40 Mev. Table IV shows the values for these ratios for n- and p-type Ge.

TABLE IV

Material	ROD - Calculated E_d= 15 ev	ROD - Calculated E_d=30 ev	ROD Measured
n-Type Ge 10 Ω-cm	1.5	1.3	1.2
n-Type Ge 20 Ω-cm	1.5	1.3	1.6
p-Type Ge 10 Ω-cm	1.4	1.2	1.7

The measured values given in the table are of the same order of magnitude as those calculated, which implies that, in spite of the very drastic effect of the low temperature annealing, the theory can still predict directions and order of magnitude for the energy dependence of radiation damage induced by electrons.

Figure 17 shows the theoretical and experimental curves. The experimental curves have been shifted such that the relative position of the points on the curve have been retained but the absolute values have not. When we analyze the data as given in Table I and Figure 17 it is seen that the 10 and 20 Ω-cm n-type germanium gives results which agree reasonably well with the 15 ev threshold theoretical curve. The 10 Ω-cm p-type material gives a slope which is greater than that of the theoretical curve.

Conclusions and Discussion for Room Temperature Bombardments

The purpose of this experiment was to make an energy dependence study of electron radiation damage to germanium. In each case for extrinsic materials the damage by electrons is energy dependent increasing slowly the higher the energy. We were unable to observe substantial differences in the damage for the samples irradiated at 12 and 25 Mev. This may have been due in part to uncertainties in flux measurements. For n-type germanium the radiation damage appears to be the same for both antimony and arsenic doping.

The carrier removal rates for n-type germanium were found to be of the order of 100 times greater than the carrier removal rates for p-type. The carrier removal rates for 10 ohm-cm n-type germanium were found to be 1.2 - 1.5 times greater than the carrier removal rates for 20 ohm-cm n-type germanium. It is possible that better agreement between theory and experiment may be obtained if a more sophisticated model than Kinchin-Pease[17] is used to determine the total number of displacements initiated by the primary knock-on. A step in this direction has been undertaken in some very recent work of Oen and Robinson[15] which departs from the fundamental assumption of Kinchin and Pease that the total primary knock-on energy causes displacements as the primary is finally stopped.

E. CARRIER CONCENTRATION AND CONDUCTIVITY FOR N-TYPE 10Ω-cm SILICON AND P-TYPE 1 Ω -cm GERMANIUM IRRADIATED AT -146°C

RESULTS AND DISCUSSION

10 ohm-cm n-type Si (Phosphorus Doped) The measured carrier concentration for this sample vs. integrated flux of 40.5 Mev electrons is plotted in figure 18. The carrier concentration decreases linearly with flux; that is, the carrier removal rate is almost constant below the maximum dose the sample received, which is about 11.8 x 10^{14} electrons/cm^2. The carrier removal rate, $dn/d\phi$, is found to be 0.27 per incident electron-cm.

In comparing measured carrier removal rates for 10Ω-cm n-type silicon irradiated at -146°C and at room temperature with 40 Mev electrons we find that the -146°C removal rate is 0.6 the removal rate at room temperature. Wertheim[16] has made measurements on silicon irradiated with 0.7 Mev electrons which led him to formulate a temperature dependent defect model. The same model was also deduced independently by MacKay and Klontz[17] at very nearly the same time with studies on electron irradiation of germanium. From Figure 1 of reference 16 (Wertheim's work) the ratio of damage for 0.7 Mev irradiation of silicon at -146°C to room temperature is 0.5 which agrees well with our findings

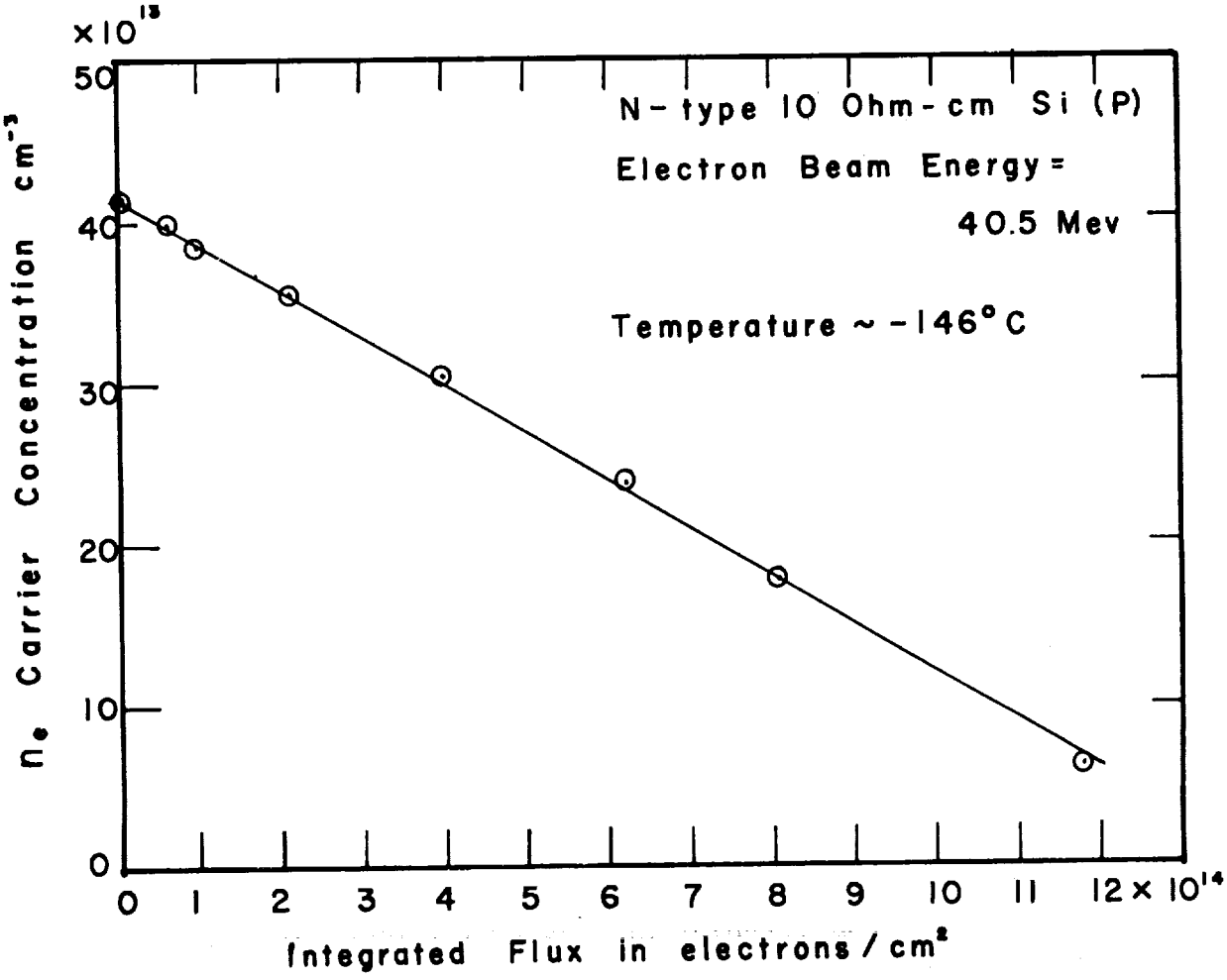
N-type 10 Ohm-cm Si (P)
Electron Beam Energy =
40.5 Mev
Temperature ~ -146°C
x10^15
50
40
30
20
10
0
n_e Carrier Concentration cm^-3
0 1 2 3 4 5 6 7 8 9 10 11 12 x 10^14
Integrated Flux in electrons / cm^2

Fig. 18

for 40 Mev electron irradiation.

An unusual change of conductivity and Hall mobility with respect to the integrated flux was observed, in which the conductivity increased rapidly at the beginning of the bombardment and passed through a maximum at a flux of 2.2×10^{14} electrons/cm^2, and then decreased with further bombardment. Also the Hall mobility increased as the dose increased.

The temperature dependence of the Hall mobility for this sample shows that the mobility of the sample before irradiation was abnormal; the impurity scattering seemed to dominate in a much higher temperature range than usual. This might be explained by some complex imperfections produced in the sample during its history before irradiation, which might cause the abnormal phenomenon in Hall mobility. Other possibilities that might explain this effect are bad contacts and surface effects.

The isochronal annealing results for this silicon sample are shown in Fig. 19. It is obvious that, from the graph of R_H vs. 1000/T (Fig. 19) there seem to be two electron trapping energy levels below the edge of the conduction band. Unfortunately, the damage is too slight to determine accurately the values of the deep energy levels. The value of the energy level closest to the conduction band is about -0.15 ev by assuming a degeneracy ratio r of 0.5, and -0.16 ev if r = 1. This trapping level is associated with the A-centers[9] ($E_t - E_c$ = -0.17 ev). The energy value of the deeper level is around -0.4 ev below the conduction band and may be the E-center found[9] for phorphorus-doped silicon.

The introduction rate of the higher energy level is about 0.11 per incident electron, and that of the deeper level is 0.16 per incident electron.

There was no annealing observed for this Si sample in the temperature range from -146°C to +30°C.

1 ohm-cm p-type Ge (Gallium doped) The measured carrier concentration of this sample vs. integrated flux of 40.5 Mev electrons is plotted in Fig. 20. The carrier removal rate, $dn/d\phi$, is found to be 0.025 per incident electron/cm. The Hall mobility was constant during the irradiation. Due to slight damage, we are not able to find defect levels. However, it is obvious that there may be an annealing peak at 180°K (see resistivity vs. 1000/T results, Fig. 21) which agrees with W. L. Brown's work[10] fairly well.

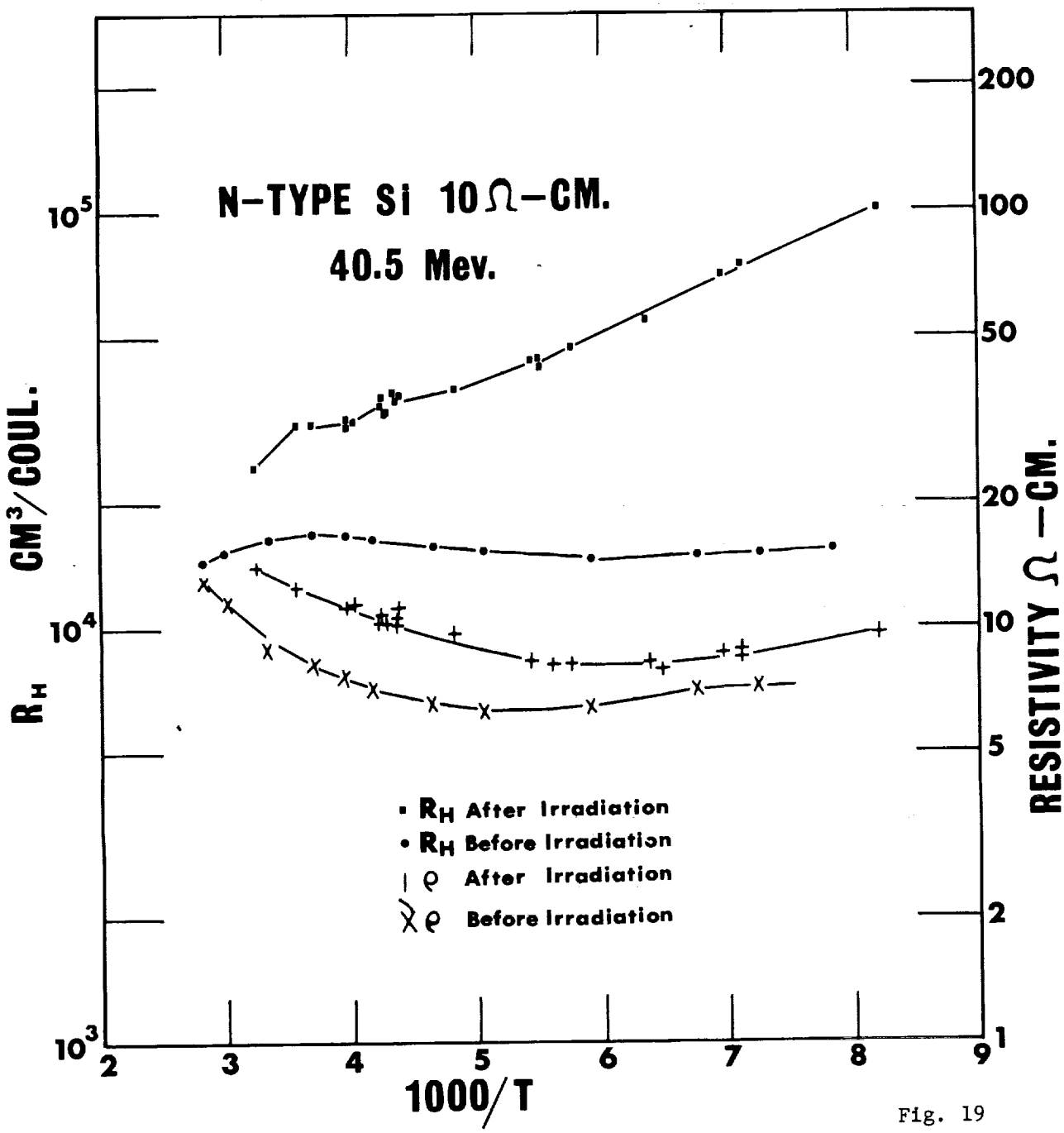
N-TYPE Si 10 Ω-CM.
40.5 Mev.
R_H CM³/COUL.
RESISTIVITY Ω-CM.
1000/T
10^5
10^4
10^3
200
100
50
20
10
5
2
1
2
3
4
5
6
7
8
9
▪ R_H After Irradiation
• R_H Before Irradiation
| ρ After Irradiation
X ρ Before Irradiation

Fig. 19

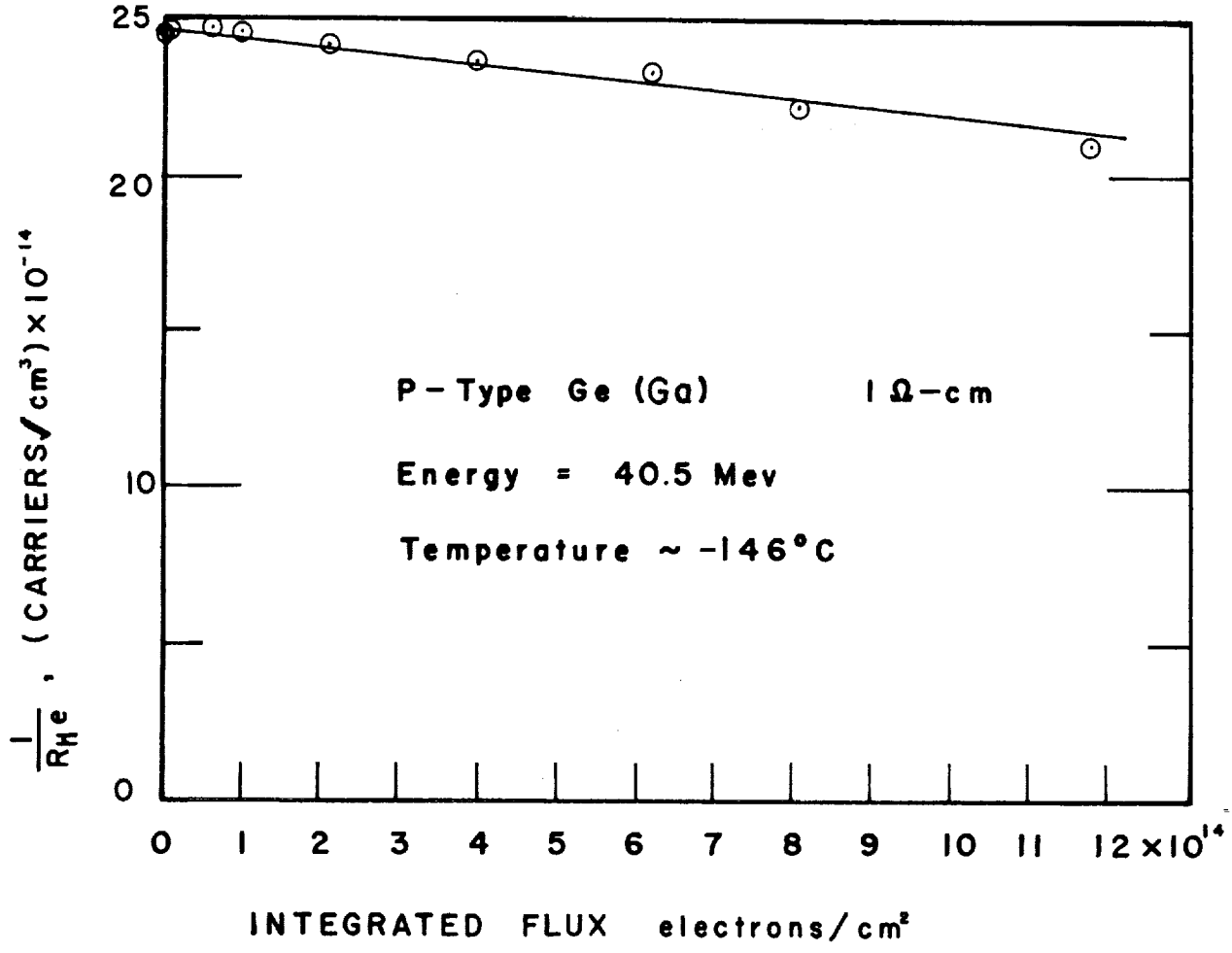
25
20
10
0
P - Type Ge (Ga) 1 Ω-cm
Energy = 40.5 Mev
Temperature ~ -146°C
$\frac{1}{R_H e}$, (CARRIERS/cm³) x 10⁻¹⁴
0 1 2 3 4 5 6 7 8 9 10 11 12 x 10¹⁴
INTEGRATED FLUX electrons/cm²

Fig. 20

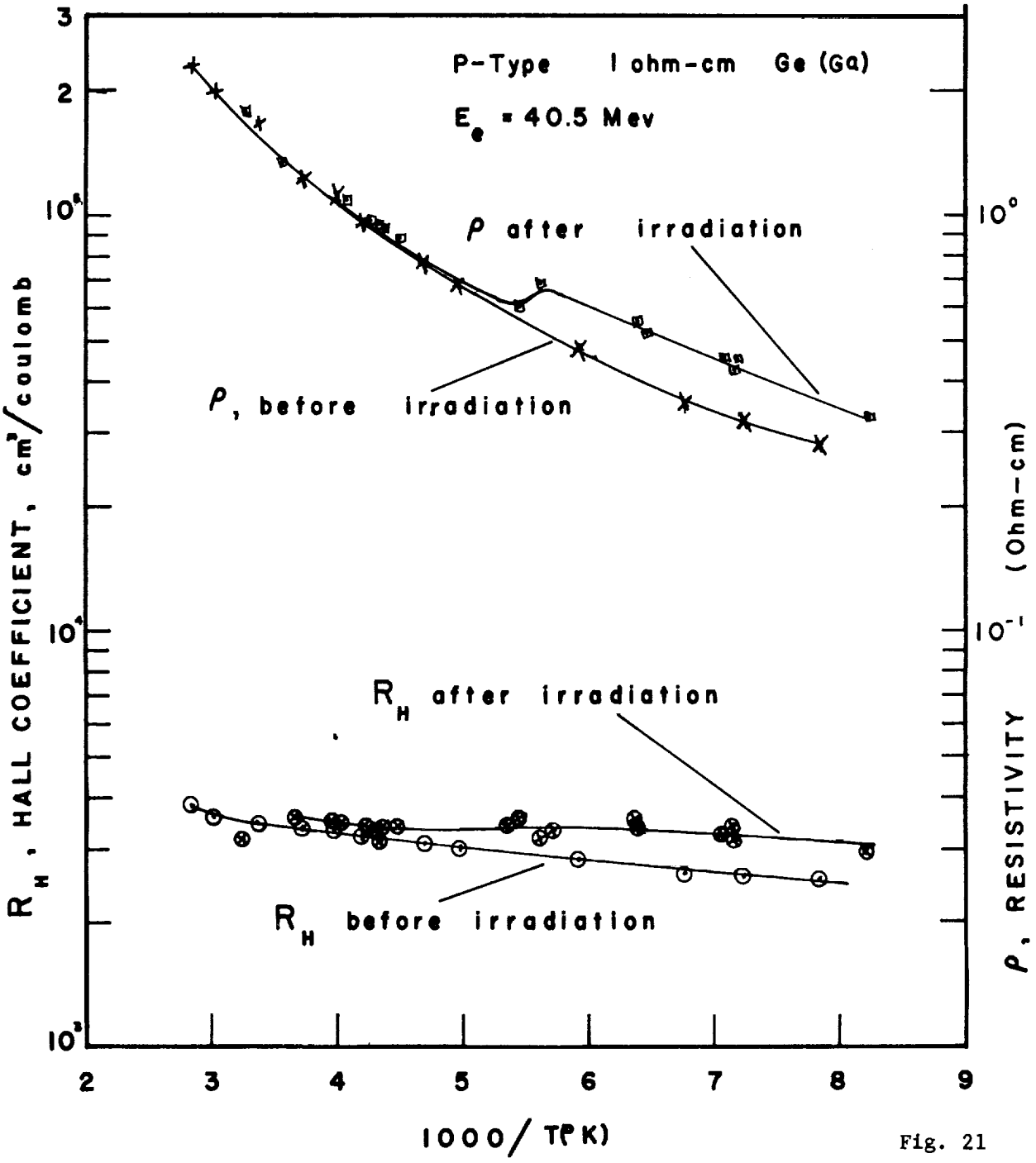
P-Type 1 ohm-cm Ge (Ga)
E_e = 40.5 Mev
ρ after irradiation
ρ, before irradiation
R_H after irradiation
R_H before irradiation
R_H, HALL COEFFICIENT, cm³/coulomb
ρ, RESISTIVITY (Ohm-cm)
1000/ T(°K)
3
2
10⁵
10⁴
10³
10°
10⁻¹
2
3
4
5
6
7
8
9

Fig. 21

F. RESULTS AND DISCUSSION OF LIFETIME MEASUREMENTS ON GERMANIUM IRRADIATED WITH 10 to 54 MEV ELECTRONS

The standard Shockley-Read result[11] for the lifetime associated with steady-state recombination at a single radiation-induced level E_r is:

$$\tau_b = \frac{\tau_{po}(n_o + n_1) + \tau_{no}(p_o + p_1)}{n_o + p_o} \qquad (1)$$

where τ_{po} is the lifetime in strongly n-type material, τ_{no} is the lifetime in highly p-type material, n_o and p_o are the equilibrium carrier concentrations and n_1 and p_1 are the carrier concentrations if the recombination level E_r coincides with the Fermi level E_f. The following approximations must be made to obtain eq. (1):

1) The injected excess carrier densities δn and δp are equal and small compared to n_o, p_o, n_1, or p_1.
2) The net capture rates of holes and electrons by recombination centers are equal.
3) The semiconductor is non-degenerate, that is, the Fermi level is several kT from both band edges.

Wertheim[12] has shown that the above also applies to transient recombination (such as is observed by the pulsed photoconductivity decay method) if the density of recombination centers is small.

The quantity τ_b represents the lifetime associated with bombardment-induced defects. The total observed lifetime τ is assumed to be given by

$$\frac{1}{\tau} = \frac{1}{\tau_b} + \frac{1}{\tau_o} \qquad (2)$$

where $1/\tau_o$ is proportional to the number of recombination centers present in an unirradiated specimen (due to chemical impurities, surface states, thermal equilibrium point defects, etc.).

Using the expression in equation (1) for τ_b, equation (2) can be approximated for various regions of Fermi level (assuming $E_r > E_i$ where E_i is the energy at the middle of the gap) as follows:

a) high-conductivity p-type ($p_o \gg n_1$):

$$\frac{1}{\tau} - \frac{1}{\tau_o} = \Delta(E_b)\,\phi\,\sigma_{ce}\,\nu_e \qquad (3)$$

b) Less strongly p-type ($n_1 \gg p_o$):

$$\frac{1}{\tau} - \frac{1}{\tau_o} = \Delta(E_b)\,\phi\,\sigma_{ch}\,v_h \exp\left[\frac{2E_i - E_f - E_r}{kT}\right] \qquad (4)$$

c) slightly n-type ($n_o \ll n_1$)

$$\frac{1}{\tau} - \frac{1}{\tau_o} = \Delta(E_b)\,\phi\,\sigma_{ch}\,v_h \exp\left[\frac{E_f - E_r}{kT}\right] \qquad (5)$$

d) high conductivity n-type ($n_o \gg n_1$):

$$\frac{1}{\tau} - \frac{1}{\tau_o} = \Delta(E_b)\,\phi\,\sigma_{ch}\,v_h \qquad (6)$$

Where v_e, v_h is the thermal velocity of electrons or holes respectively, ϕ is the integrated electron flux, and σ_{ch}, σ_{ce} is the capture cross section of a defect for holes or electrons respectively.

In obtaining eqs. 3-6 we have assumed that recombination centers are introduced uniformly with flux of electrons of energy E_b with a probability $\Delta(E_b)$ per unit path through the sample. Thus N_r, the concentration of recombination centers, as a function of flux is just $\Delta(E_b)\,\phi$. Similar expressions hold for $E_r < E_i$. If recombination centers are introduced uniformly with flux, then a plot of $1/\tau - 1/\tau_o$ vs. flux will be a straight line, as long as E_f is unchanged. The constancy of E_f also insures that the contribution to τ_o of chemical impurities will be unchanged with irradiation.

Plots of $1/\tau - 1/\tau_o$ vs. total flux are presented in Figs. 22, 23, and 24 for indium-, arsenic-, and antimony-doped samples of germanium respectively. Experimental curves extending into the negative flux axis indicate errors in dosimetry. Error bars are assigned taking $\pm$ 5% as the error in all lifetime measurements.

The best straight line fits were obtained from the 40 ohm-cm samples due to the high initial lifetime. In general, bombardments were terminated before changes in conductivity occurred, so that subsequent annealing experiments would yield information strictly relating to recombination centers.

It is seen that the plots yield straight lines up to fluxes of from 10^{13} e/cm^2 for 3.5 Ω cm to 5 X 10^{13} e/cm^2 for the purer 20 and 40 ohm-cm samples. This is in accord with observations that the carrier concentration changes with smaller doses for low-resistivity material than for high-resistivity

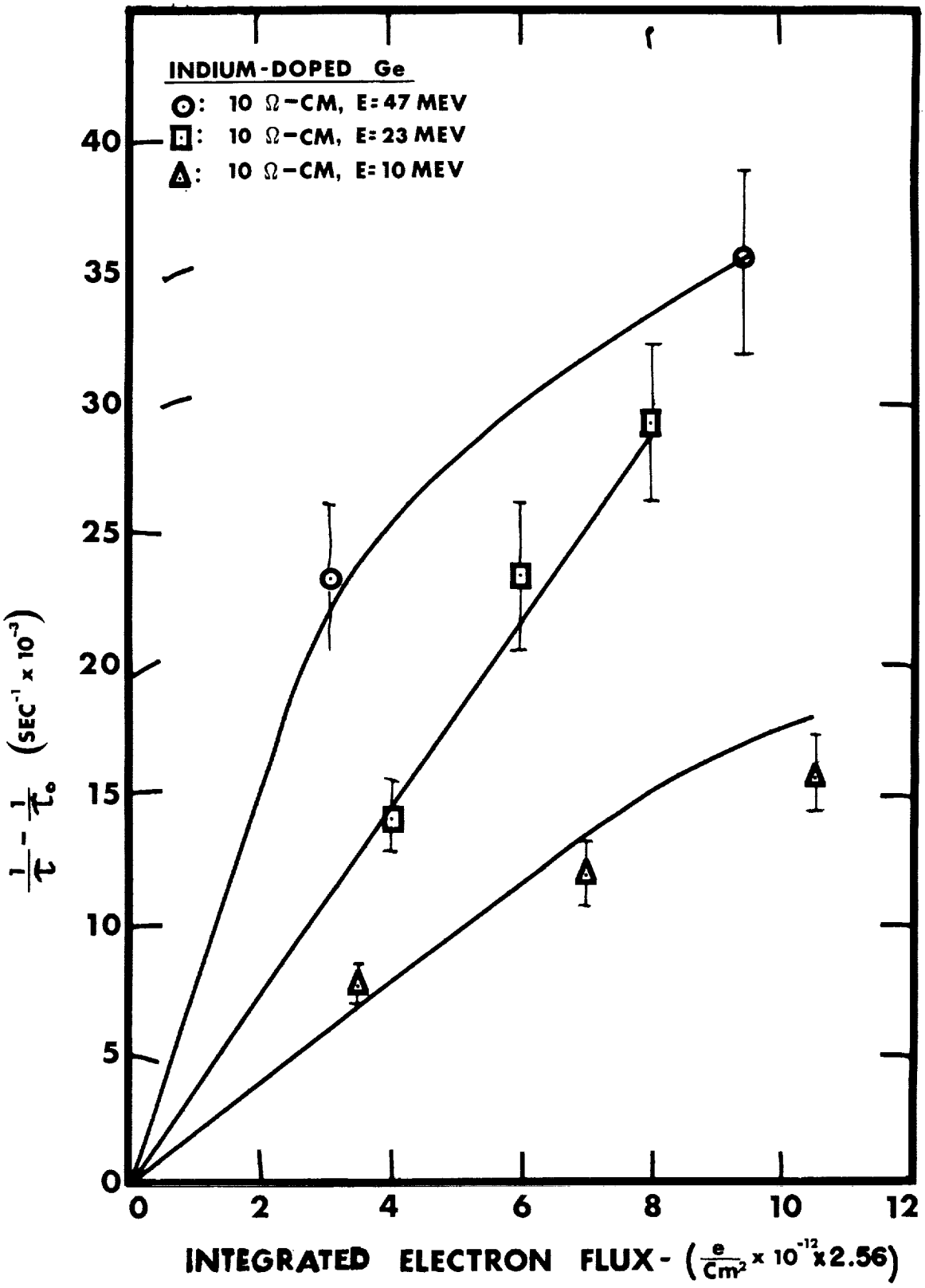
INDIUM-DOPED Ge
⊙: 10 Ω-CM, E=47 MEV
⊡: 10 Ω-CM, E=23 MEV
△: 10 Ω-CM, E=10 MEV
$\frac{1}{\tau} - \frac{1}{\tau_o}$ (SEC^{-1} x 10^{-3})
0
5
10
15
20
25
30
35
40
0
2
4
6
8
10
12
INTEGRATED ELECTRON FLUX - ($\frac{e}{cm^2}$ x 10^{-12} x 2.56)

Fig. 22

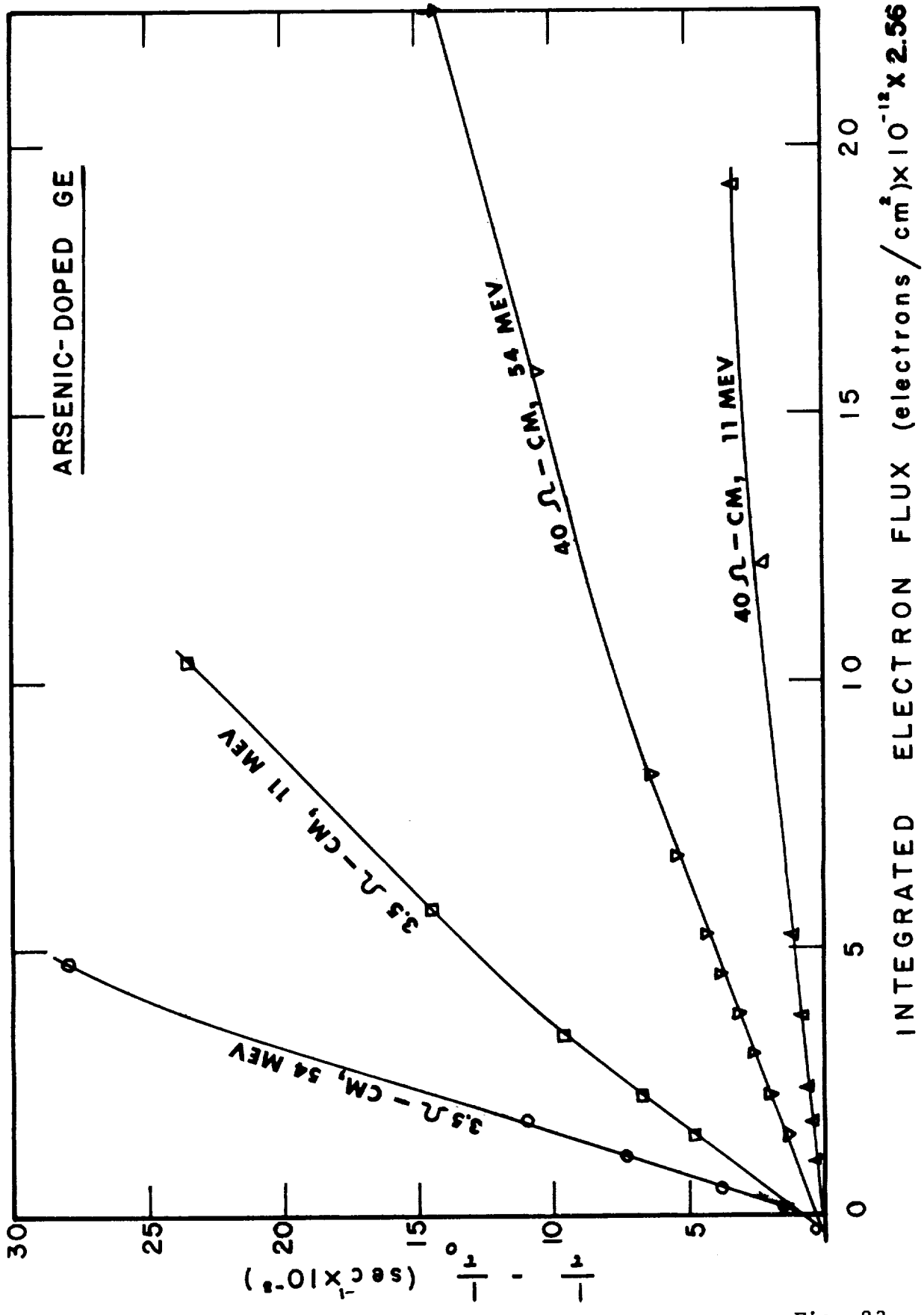
ARSENIC-DOPED GE
40 Ω-CM, 54 MEV
40 Ω-CM, 11 MEV
3.3 Ω-CM, 11 MEV
3.3 Ω-CM, 54 MEV
INTEGRATED ELECTRON FLUX (electrons/cm²)X10⁻¹²X 2.56
1/τ - 1/τ₀ (sec⁻¹X10⁻⁸)
0
5
10
15
20
25
30

Fig. 23

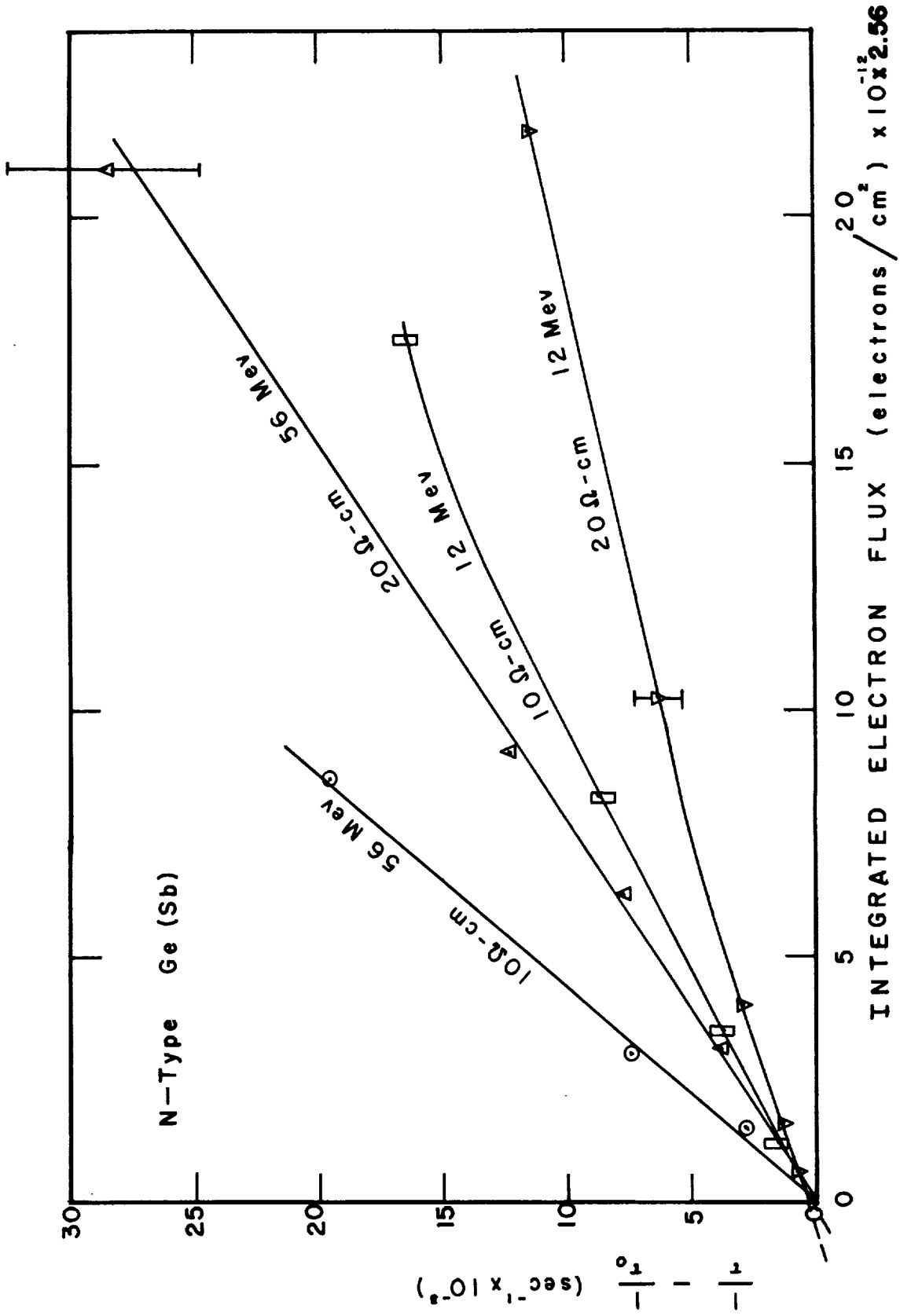
N—Type Ge (Sb)
56 Mev
20Ω-cm
12 Mev
10Ω-cm
12 Mev
20Ω-cm
56 Mev
10Ω-cm
INTEGRATED ELECTRON FLUX (electrons/cm²) x 10⁻¹² x 2.56
0
5
10
15
20
30
25
20
15
10
5
0
1/τ - 1/τ₀ (sec⁻¹ x 10⁻⁸)

Fig. 24

material. As mentioned before, the p-type samples are doubtful; they are included in this report only to illustrate trends.

These figures represent only the first 1/3 to 1/8 of the total bombardments, since the initial slopes of the straight line portions are of immediate interest. The slopes of the plots decreased with flux in all cases, as predicted and experimentally verified by Wertheim for Si[12]. Total fluxes were kept low enough to avoid approaching the maximum in the plot of $1/\tau$ vs. flux observed by Wertheim.

In Fig. 25 are plotted the slopes of the straight lines of Figs. 22, 23 and 24 vs. E_b, the bombardment energy. The curves are extended to zero damage at E_b = 360 keV, which is the observed threshold for lifetime change with electron bombardment of Ge[2]. Included are four points obtained by other investigators noted on the graph.

It should be mentioned in passing that although the resistivities quoted are nominal, all samples of a given type were cut from the same ingot. The axial distance along the ingot from which each sample was taken varied by no more than 3mm.

Figure 26 represents the slopes of Figs. 22, 23 and 24 vs. carrier concentration. The solid line for 1.0 MeV is from reference 13. Differentiating eqs. 4 and 5 with respect to ϕ and taking logs shows that, for slightly n- or p-type material, Figure 25 should be linear in $E_f - E_v$ (or $\ln n_o/n_i$ with slope unity. This is true for 1.0 and 12 MeV but not for 55 MeV, indicating that a single level defect is produced at 1.0 and 10 MeV but not at 55 MeV. The higher-energy situation could possibly be fitted by more than one combination level with different minority carrier capture cross-sections, but this has not been attempted.

An estimate of the displacement cross-section for 12 MeV electrons has been obtained. If one assumes that the defects formed at 1 Mev and 12 Mev have identical Tce, Tch and Er, then from Eqs. (4) and (5) the minima of the curves in Fig. 26 are directly proportional to $\Delta(E_b)$. The observed ratio Δ (12 MeV)/ Δ (1 MeV) is 88. Using the result of Ref. 13 (Δ (1 MeV) = .175 cm^{-1}) gives Δ(12 MeV) = 15.4 cm^{-1}.

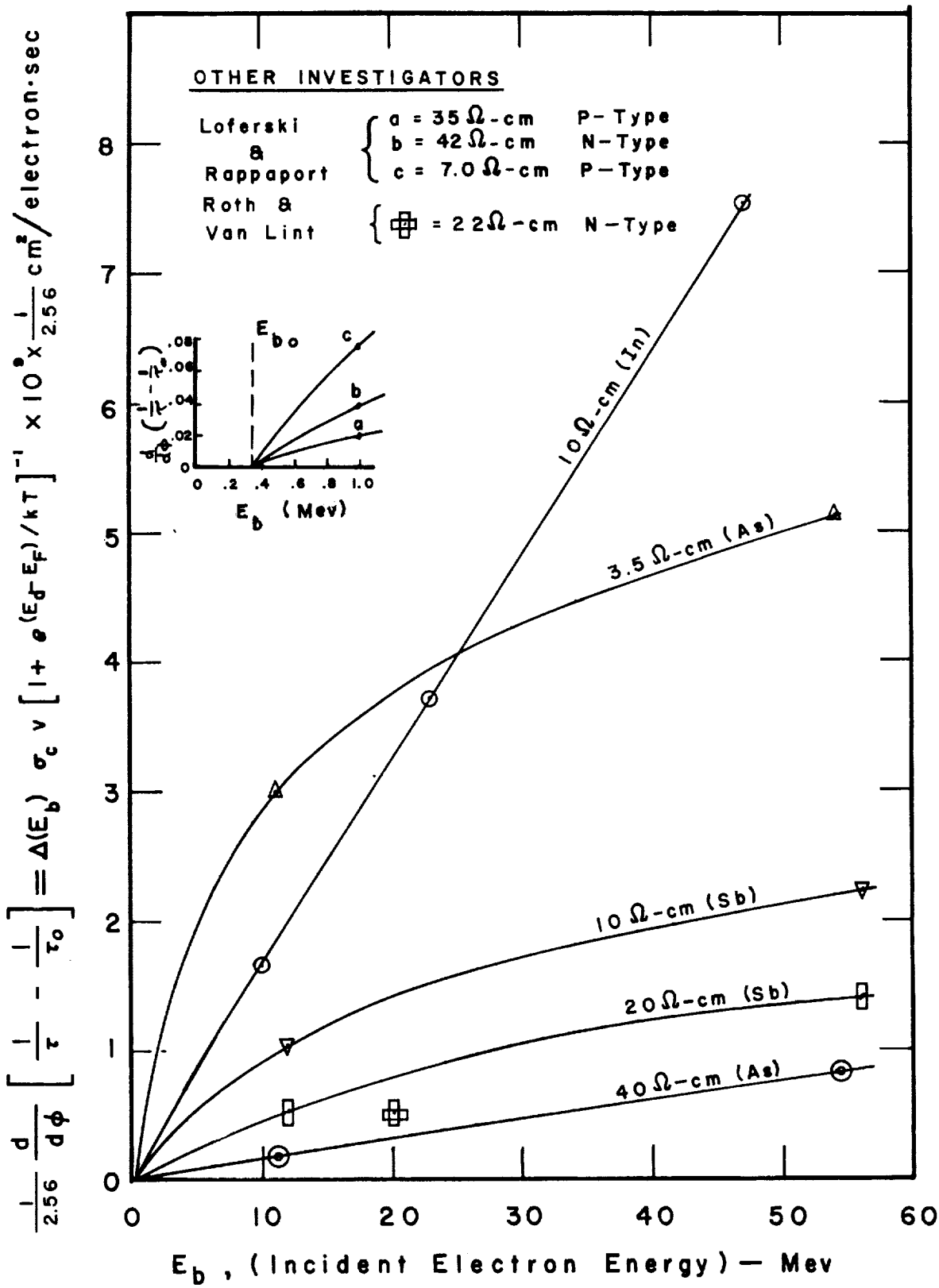
OTHER INVESTIGATORS
Loferski & Rappaport
a = 35 Ω-cm P-Type
b = 42 Ω-cm N-Type
c = 7.0 Ω-cm P-Type
Roth & Van Lint
= 22Ω-cm N-Type
10 Ω-cm (In)
3.5 Ω-cm (As)
10 Ω-cm (Sb)
20 Ω-cm (Sb)
40 Ω-cm (As)
E_bo
E_b (Mev)
E_b , (Incident Electron Energy) — Mev

-60-

Fig. 25

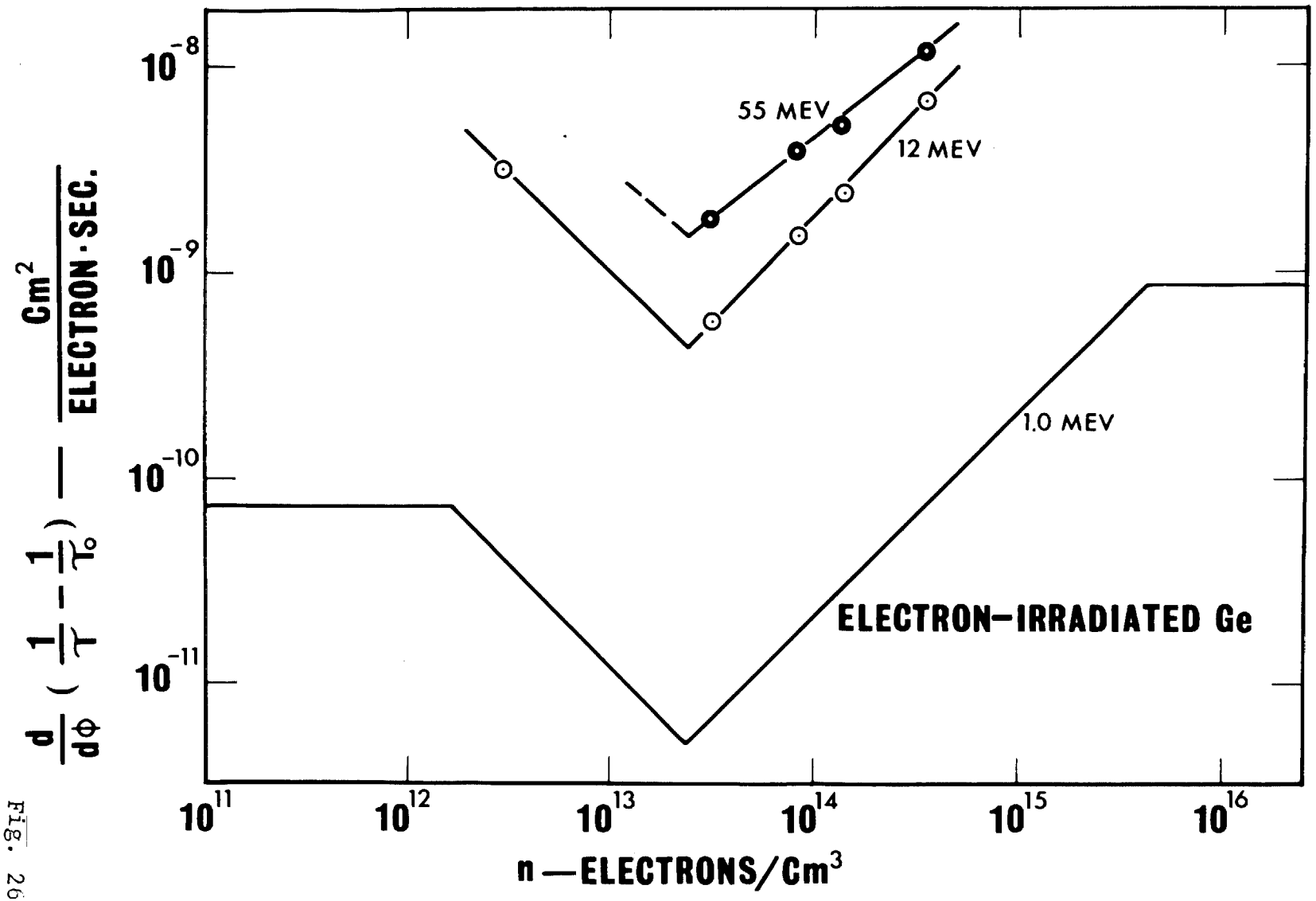
$\frac{d}{d\Phi}\left(\frac{1}{\tau}-\frac{1}{\tau_o}\right)$ — $\frac{Cm^2}{ELECTRON \cdot SEC.}$
10^{-8}
10^{-9}
10^{-10}
10^{-11}
55 MEV
12 MEV
1.0 MEV
ELECTRON–IRRADIATED Ge
10^{11}
10^{12}
10^{13}
10^{14}
10^{15}
10^{16}
n — ELECTRONS/Cm^3

Fig. 26

Comparing these with the results of ref. 13 indicates that $\Delta(E_b)$= 5.36 cm^{-1} at 10 meV, and the corresponding atomic displacement cross-section is 113 barns. The corresponding values at 1.0 Mev are 0.175 cm^{-1} and 3.7 barns.

The position of the recombination level E_r is very sensitive to the values of $\sigma_{ch}v_h$ and $\sigma_{ce}v_e$, as may be seen by differentiating eqs. 4 and 5. From our data it is not possible to determine whether the position of the level is the same at 10 MeV as at 1.0 MeV since we did not irradiate any highly extrinsic samples, and thus cannot determine the capture cross-sections accurately enough. Annealing experiments will be performed on these samples in the near future which will hopefully yield this information.

In Table V are presented computed values of $\Delta(E_b)$ for E_b = 10 MeV for various thresholds E_d in germanium. These values are from the same computation which gave the theoretical curves in Fig. 17. It is seen that the experimental estimate of 11.4 displacements/cm is in agreement with a displacement threshold of about 15 eV. Cahn[8] has shown that recent electron irradiations by McKay at 2.5 to 5.0 MeV can be explained better if E_d = 30 ev rather than 15 ev.

TABLE V

(E_b = 10 Mev)

E_d (eV)	(computed) displacements/cm
15	15.6
20	11.0
25	8.4
30	6.7
35	5.6

We sincerely acknowledge the RPI Linac crew, namely William McRoberts, Judson Snyder, and David Kraus for their excellent help in running the Linac during our experiments.

V. PLANS FOR FUTURE EXPERIMENTS

The future experiments most pertinent to the results given in this report are the detailed temperature dependence and annealing measurements on many of the samples irradiated at room temperature. In order to derive the maximum amount of information about the radiation damage process (eg, defect energy levels, annealing characteristics) we have found that extremely careful and time consuming experiments must be performed. We therefore find it necessary to build another facility for measuring conductivity and Hall coefficient from 75°K up to 600°K. It is anticipated that the above experiments will allow comparisons and correlations to be made between high-energy proton and electron damage.

An apparatus has been designed which will be capable of measuring successively the conductivity, Hall coefficient and minority carrier lifetime from 75°K up to 600°K on the same sample. The apparatus will be built inside a mobile frame thus allowing one to carry on irradiations in the Linac target room and removing the apparatus outside the target room for the lengthy post-irradiation experiments. Since the apparatus is highly specialized the design is being submitted to vendors outside RPI for bids.

Cold temperature ($\sim 80°K$) electron irradiation (20-40 Mev) experiments on silicon and germanium are being prepared now for a Linac run late in November 1963. The purpose of these cold irradiations is to study which defect levels are excited in silicon and germanium and moreover, to search for occurrence of annealing stages in the temperature range 80 - 500°K.

Samples of silicon and germanium are to be prepared for at least one more fairly extensive run at the Harvard University proton cyclotron during the next six month period in which the precise experiment to be performed is based on the proton results gathered thus far.

A new search for the defect energy levels induced in heavily irradiated ($\gtrsim 10^{18} e/cm^2$) silicon by infra-red absorbtivity measurements will be made. It is felt that the similarity of our high-energy radiation damage to what is observed at low energy should also be observable using infra-red as a probe for defects.

Although in the planning stages at present, we wish to state briefly that our program will include at least one irradiation with high-energy electrons in which we shall attempt to observe the enhancement of diffusion in germanium or silicon under the influence of radiation.

Well known work by Dienes and Damask indicates that the diffusion coefficient in the temperature range 0 - 400°C is greatly enhanced under the action of a radiation field having sufficiently high-energy to create vacancies and interstitials.

In conclusion, we shall continue in our attempts to find theoretical methods for analysis of our data, and wherever possible use computer calculations for complicated numerical problems.

G. Figure Captions

Fig. 1 Carrier Removal Rate vs. Electron Energy for 1 and 10 Ω cm n-type Silicon and 10 Ω cm p-type Silicon Irradiated at 25°C.

Fig. 2 Conductivity vs. Integrated Electron Flux for 10 Ω cm p-type Silicon Irradiated at 25°C.

Fig. 3 Carrier Concentration (using $R_H = \frac{1}{ne}$) vs. Integrated Electron Flux for 1 Ω cm n-type Silicon Irradiated with 17 and 35 Mev Electrons at 25°C.

Fig. 4 Conductivity vs. Integrated Electron Flux for 1 Ω cm n-type Silicon Irradiated with 17 and 35 Mev Electrons at 25°C.

Fig. 5 Conductivity vs. Integrated Electron Flux for 10 Ω cm n-type Ge (Antimony doped) Irradiated with 12, 25, and 54 Mev electrons at 25°C.

Fig. 6 Carrier Concentration (using $R_H = \frac{1}{ne}$ vs. Integrated Electron Flux for 10 Ω cm n-type Ge (Antimony doped) Irradiated with 12, 25 and 54 Mev Electrons at 25°C.

Fig. 7 Hall Mobility vs. Integrated Electron Flux for 10 Ω cm n-type Ge (Antimony doped) Irradiated with 12, 25 and 54 Mev Electrons at 25°C.

Fig. 8 Conductivity vs Integrated Electron Flux for 20 Ω cm n-type Ge (Antimony doped) Irradiated with 12, 35.7 and 54 Mev Electrons at 25°C.

Fig. 9 Carrier Concentration (using $R_H = \frac{1}{ne}$ vs. Integrated Electron Flux for 20 Ω cm Ge (Antimony doped) Irradiated with 12, 25 and 54 Mev Electrons at 25°C.

Fig. 10 Hall mobility vs. Integrated Electron Flux for 20 Ω cm n-type Ge (Antimony doped) Irradiated with 12 and 54 Mev Electrons at 25°C.

Fig. 11 Conductivity Hall Coefficient vs. Integrated Electron Flux for 35 Ω cm n-type Ge (Arsenic doped) Irradiated with 35.7 and 54 Mev Electrons at 25°C.

Fig. 12 Conductivity vs. Integrated Electron Flux for a 10 Ω cm Arsenic Doped and a 10 Ω cm Antimony Doped n-type Germanium Irradiated with 12 Mev Electrons at 25°C.

Fig. 13 Carrier Concentration (using $R_H = \frac{1}{ne}$) vs. Integrated Electron Flux for a 10 Ω cm Arsenic Doped and a 10 Ω cm Antimony Doped n-type Germanium Irradiated With 12 Mev Electrons at 25°C.

Fig. 14 Hall Mobility vs. Integrated Electron Flux for Arsenic and Antimony Doped 10 Ω cm Germanium Irradiated with 12 Mev Electrons at 25°C.

Fig. 15 Conductivity vs. Integrated Electron Flux for 10 Ω cm p-type Germanium (Indium Doped) Irradiated with 12, 25 and 40 Mev Electrons at 25°C.

Fig. 16 Carrier Concentration (using $R_H = \frac{1}{pe}$) vs. Integrated Electron Flux for 10 Ω cm p-type Germanium Irradiated with 12, 25, and 40 Mev Electrons at 25°C.

Fig. 17 Comparison of Calculated Number of Displacements to the Adjusted Carrier Removal Rates (see Text) vs. a Function of Electron Energy for n- and p-type Germanium Irradiated at 25°C.

Fig. 18 Carrier Concentration (using $R_H = \frac{1}{ne}$) vs. Integrated Flux for 10 Ω cm n-type Silicon Irradiated with 40.5 Mev Electrons at -146°C.

Fig. 19 Hall Coefficient and Resistivity of 10 Ω cm n-type Silicon vs. $\frac{1000}{T(°K)}$ before Irradiation by 40.5 Mev Electrons at -146°C and after annealing from -146°C to 30°C.

Fig. 20 Carrier Concentration (using $R_H = \frac{1}{pe}$) vs. Integrated Flux for 1 Ω cm p-type Germanium Irradiated with 40.5 Mev Electrons at -146°C.

Fig. 21 Hall Coefficient and Resistivity of 1 Ω cm p-type Germanium vs. $\frac{1000}{T(°K)}$ before Irradiation by 40.5 Mev Electrons at -146°C and after annealing from -146°C to 30°C.

Fig. 22 Difference in minority Carrier Lifetime vs. Integrated Flux for 10 Ω cm p-type Germanium (Indium Doped) Irradiated with 10 to 47 Mev Electrons at 25°C (τ_o = Initial Carrier Lifetime).

Fig. 23 Difference in Minority Carrier Lifetime vs. Integrated Flux for 3.5 and 40 Ω cm n-type Germanium (Arsenic Doped) Irradiated with 11 and 54 Mev Electrons at 25°C. (τ_o = Initial Carrier Lifetime.)

Fig. 24 Difference in Minority Carrier Lifetime vs. Integrated Flux for 10 and 20 Ω cm n-type Germanium (Antimony Doped) Irradiated with 12 and 56 Mev Electrons at 25°C. (τ_o = Initial Carrier Lifetime)

Fig. 25 Slope of Minority Carrier Lifetime Electron Flux Curves vs. Incident Electron Energy for n- and p-type Germanium. (Dopant and Resistivity shown on curves).

Fig. 26 Slope of Minority Carrier Lifetime Electron Flux Curves vs. Initial Carrier Concentration, n_o, for 1, 10, and 55 Mev Irradiation of n- and p-type Germanium.

H. References

1. G. K. Wertheim, J. App. Phys. 30, 1166 (1959).
2. J. J. Loferski and P. Rappaport, Phys. Rev. 111, 432 (1958).
3. M. V. Sullivan and J. H. Eigler, J. Electrochem. Soc. 104, 226 (1957).
4. O. L. Curtis, Jr. and J. H. Crawford, Jr., "The Carrier-Recombination Behavior and Annealing Properties of Radiation-Induced Recombination Centers in Germanium," ORNL-3108 UC-34-Physics (May 1961).
5. Navon, Bray and Fan, Proc. I. R. E. 40, 1342 (1952).
6. G. W. Simon, J. M. Denney and R. G. Downing, Phys. Rev. 129, 2454 (1963).
7. F. Seitz and J. S. Koehler, Solid State Physics, Vol. 2 (1956).
8. J. H. Cahn, J. App. Phys. 30, 1310 (1959).
9. G. D. Watkins, J. W. Corbett and R. M Walker, J. Appl. Phys. 30, 1198 (1959).
   G. D. Watkins and J. W. Corbett, Phys. Rev. 121, 1001 (1961).
10. W. L. Brown, W. M. Augustyniak, and T. R. Waite, J. Appl. Phys. 30, 1258 (1959).
11. W. Shockley and W. T. Read, Phys. Rev. 87, 835 (1952).
12. G. K. Wertheim, Phys. Rev., 109, 1086 (1958).
13. J. J. Loferski and P. Rappaport, J. Appl. Phys. 30, 1181 (1959).
14. G. K. Wertheim, Phys. Rev. 105, 1730 (1957).
15. O. S. Oen and M. T. Robinson, Appl. Phys. Letters 2 #4, 83 (1963).
17. J. W. MacKay and E. E. Klontz, J. Appl. Phys. 30, 1269, (1959).
16. G. K. Wertheim, Phys. Rev. 115, 568 (1959).

NASA-Langley, 1964 F-212